

# Beyond Local Independence: High-Dimensional Latent Class Graphical Models with Shared Block Structure

Seunghyun Lee and Yuqi Gu

Department of Statistics, Columbia University

## Abstract

Latent class models are central tools for multivariate categorical data from heterogeneous populations, but their standard local-independence assumption is often unrealistic in modern high-dimensional applications. We propose a high-dimensional latent class graphical model for ordinal responses with block-structured local dependence. The model retains the interpretability and parsimony of classical latent class analysis by imposing a shared block partition of variables, while allowing class-specific graphical dependence within each block. We develop a scalable three-step estimator that first recovers latent classes by spectral clustering of a flattened response matrix, then estimates class-specific latent covariance matrices and aggregates them to recover the shared block partition, and finally estimates sparse within-block precision matrices. We establish finite-sample error bounds for clustering, covariance estimation, block recovery, and precision-matrix estimation, yielding end-to-end consistency of all model components under high-dimensional scaling. Simulations demonstrate accurate recovery of latent classes, the shared block partition, and class-specific dependence graphs with scalable computation. Applications to American National Election Studies survey data and HapMap3 genotype data show that the method uncovers interpretable local dependence structures while accounting for latent heterogeneity.

**Keywords:** Latent class models; Local dependence; High-dimensional graphical models; Block structure; Gaussian copula

## 1 Introduction

Modern social-science and biomedical studies often collect high-dimensional ordinal or categorical measurements in the presence of unobserved population heterogeneity. Latent class models (LCMs) are widely used mixture models for such data: each individual belongs to a

---

Emails: s14963@columbia.edu, yuqi.gu@columbia.edu

latent class, and the class-specific multivariate response distributions capture heterogeneity across latent subpopulations. Since their introduction in Lazarsfeld (1950), LCMs have become standard tools for clustering and modeling multivariate categorical responses in social science, education, and related fields (Magidson et al., 2020; Vermunt and Magidson, 2002; Wang and Hanges, 2011; Korpershoek et al., 2015; Lyu et al., 2025; Lyu and Gu, 2026).

A central simplifying assumption in traditional LCMs is *local independence*: conditional on the latent class, the observed multivariate responses are mutually independent. This assumption makes the model parsimonious and computationally tractable, but it is often too restrictive in applications, especially for high-dimensional responses. For example, in public opinion surveys, items concerning the same political topic, using similar wording, or appearing in related questionnaire modules may remain dependent even after conditioning on a respondent’s latent political subgroup. In genetic SNP genotype data, nearby genetic markers often exhibit dependence due to *linkage disequilibrium*, producing block-like correlation patterns along the genome (Barrett et al., 2005; Gabriel et al., 2002). In both examples, local dependence arises from common, interpretable groupings of variables. Ignoring such dependence can distort parameter estimates and latent class assignments, as well as limit scientific interpretation (Vacek, 1985; Hageaars, 1988).

This challenge of relaxing local independence is further amplified in modern high-dimensional data with an *unknown dependence* structure. As the number of responses  $J$  grows, estimating the dependence structure among the  $J$  variables becomes computationally challenging. Existing approaches to local dependence in LCMs provide important modeling tools, but they are typically developed for lower-dimensional settings, rely on prespecified or heavily parameterized (unstructured) dependence structures, and do not provide statistical guarantees (Hageaars, 1988; Qu et al., 1996; Lee et al., 2020, 2022; Mazaheri et al., 2023, see Supplement A for a detailed discussion). Conversely, high-dimensional Gaussian-copula graphical models are designed to learn dependence among variables (Liu et al., 2012; Danaher et al., 2014; Guo et al., 2015; Fan et al., 2017; Feng and Ning, 2019), but generally do not address unknown heterogeneous latent classes. Thus, there remains a need for principled statistical

methodology that jointly learns latent heterogeneity and structured local dependence from high-dimensional ordinal responses.

Motivated by this gap, we propose a high-dimensional latent class graphical model with shared block structure. Conditional on the latent class, ordinal responses are modeled through a latent Gaussian copula, whose covariance matrix is block diagonal after a shared permutation of variables. The shared block partition captures interpretable groups of locally dependent variables, while the within-block graphical structure is allowed to vary across latent classes. Going back to the survey example, this block structure represents item groups corresponding to different survey topics. Within each block, the dependence structure is allowed to vary flexibly across classes, capturing class-specific heterogeneity. Thus, our modeling strategy provides a middle ground between the classical local independent LCM and an unrestricted mixture of graphical models, where the latter is difficult to estimate and interpret in high dimensions.

Methodologically, we introduce a computationally efficient three-step estimation pipeline to learn the shared block structure as well as all other model components (such as the latent classes and latent covariance/precision matrices) in an unsupervised manner. First, we use the low-rank structure of the response matrix and apply *spectral clustering* of the flattened data matrix to learn the latent class labels. Second, within each estimated latent class, we estimate the latent covariance matrix using pairwise *polychoric correlations*, and then aggregate the resulting sparsity patterns across classes to recover the shared block partition. Finally, after the blocks have been learned, we estimate the finer conditional dependence structures within them through sparse *precision-matrix estimation*. Each step is computationally feasible for large  $J$ , avoiding the full likelihood optimization that would be required by an unrestricted locally dependent LCM. Overall, this yields an unsupervised, scalable, and theoretically justified approach for learning latent classes, shared block structure, and class-specific graphical dependence in high dimensions. Importantly, our theory provides end-to-end guarantees: we derive non-asymptotic error bounds for each estimation stage and establish consistency of the complete pipeline under a high-dimensional scaling.

Simulation studies show that the proposed method accurately recovers latent classes, shared block structures, and class-specific precision matrices across a range of high-dimensional settings. We demonstrate the proposed methodology in two applications that motivate the study: public-opinion survey responses from the American National Election Studies and SNP genotype data from HapMap3. In the survey application, the learned blocks correspond to interpretable item groups such as political engagement and racism. In the genotype application, the method detects dependent blocks among SNPs in the presence of unknown, heterogeneous subpopulations. Together, these examples illustrate that the proposed framework can uncover interpretable block dependence structures while accounting for latent heterogeneity.

The remainder of this paper is organized as follows. Section 2 proposes the block-dependent latent class model after reviewing the standard latent class model. Section 3 details the three-step estimation methodology along with theoretical guarantees and implementation details. Section 4 conducts simulations to evaluate the statistical performance and computational efficiency of the proposed method. Section 5 demonstrates the real-world utility of our method by applying it to two diverse real datasets, one from social science surveys and one from genetics. Section 6 concludes the paper by discussing avenues for future research. The R code for the proposed method is available at <https://github.com/seunghyun-stats/Block-dependent-LCM>.

**Notation.** For any positive integer  $K$ , set  $[K] := \{1, \dots, K\}$ . Let  $\Delta^K$  denote the  $K$ -dimensional probability simplex. Given a finite set  $A$ , let  $\mathcal{S}_A$  denote the set of permutations on  $A$ . Let  $\Phi/\phi$  denote the c.d.f./p.d.f. of the standard normal, respectively. Similarly, let  $\Phi_2$  denote the c.d.f. of a bivariate normal  $(X_1, X_2)^\top$  where  $X_1, X_2$  have standard normal marginals and correlation  $\rho$ , i.e.,  $\Phi_2(u, v, \rho) := \mathbb{P}(X_1 \leq u, X_2 \leq v)$ . For a  $J \times J$  matrix  $\mathbf{M}$ , denote the operator norm (spectral norm) as  $\|\mathbf{M}\|$ . Denote the entry-wise maximum norm as  $\|\mathbf{M}\|_{\max} := \max_{j, j' \in [J]} |\mathbf{M}_{(j, j')}|$ . For a (not necessarily square) matrix  $\mathbf{M}$ , denote its  $k$ th largest singular value as  $\sigma_k(\mathbf{M})$ . Throughout the paper,  $c_1, c_2, \dots$  will denote constants

whose exact values may vary across contexts.

## 2 Model Setup

### 2.1 Latent class models

We first introduce the standard LCM framework. For  $N$  individuals and  $J$  ordinal items, let  $R_{i,j} \in [C_j]$  denote the response of individual  $i$  to item  $j$ , where  $C_j \geq 2$  is the number of categories for item  $j$ . Denote the aggregate  $N \times J$  response matrix as  $\mathbf{R}$ .

Each individual has a latent class  $Z_i \in [K]$ , generated with proportion parameter  $\boldsymbol{\pi} = (\pi_1, \dots, \pi_K)^\top \in \Delta^K$ :

$$Z_i \stackrel{i.i.d.}{\sim} \text{Categorical}(\boldsymbol{\pi}). \tag{1}$$

In other words, we assume  $\mathbb{P}(Z_i = k) = \pi_k$ . Conditional on the latent class  $Z_i$ , the item responses  $R_{i,j}$  are generated independently, i.e.,  $R_{i,1} \perp\!\!\!\perp \dots \perp\!\!\!\perp R_{i,J} \mid Z_i$ :

$$R_{i,j} \mid (Z_i = k) \stackrel{ind.}{\sim} \text{Categorical}(\boldsymbol{\theta}_{j,k}), \quad \forall k \in [K], \tag{2}$$

where  $\boldsymbol{\theta}_{j,k} = (\theta_{j,1,k}, \dots, \theta_{j,C_j,k})^\top \in \Delta^{C_j}$  is the class-specific probability mass function for item  $j$ . These vectors differ across  $k$ , reflecting heterogeneity across latent classes.

As discussed in the introduction, despite its modeling convenience, this *local independence* assumption in (2) is often violated in practice. Next, we describe the proposed model that allows structured conditional dependence.

### 2.2 Block-dependent latent class models

We define the model through the generative process for  $\mathbf{R}$ . The usual LCM is generalized by viewing ordinal responses as discretizations of a latent Gaussian; see Figure 1 for a graphical illustration. Given a latent class  $Z_i = k$  as in (1), generate a latent Gaussian vector  $\mathbf{X}_i = (X_{i,1}, \dots, X_{i,J})^\top$ :

$$\mathbf{X}_i \mid Z_i = k \stackrel{i.i.d.}{\sim} \mathcal{N}_J(\mathbf{0}, \boldsymbol{\Sigma}_k). \tag{3}$$

Here, without loss of generality, assume  $\text{diag}(\boldsymbol{\Sigma}_k) = \mathbf{1}_J$  for all  $k \in [K]$ . The observed ordinal responses are obtained by thresholding  $X_{i,j}$  at  $\boldsymbol{\Delta}_{j,k} = (\Delta_{j,1,k}, \dots, \Delta_{j,C_j-1,k})^\top$ :

$$R_{i,j} = \begin{cases} 1 & \text{if } X_{i,j} < \Delta_{j,1,k}, \\ 2 & \text{if } \Delta_{j,1,k} \leq X_{i,j} < \Delta_{j,2,k}, \\ \dots, & \\ C_j & \text{if } \Delta_{j,C_j-1,k} \leq X_{i,j}. \end{cases} \quad (4)$$

Here  $\Delta_{j,1,k} < \dots < \Delta_{j,C_j-1,k}$ , so larger latent Gaussian values produce larger ordinal responses. Write  $\boldsymbol{\Delta}_k := (\boldsymbol{\Delta}_{1,k}^\top, \dots, \boldsymbol{\Delta}_{J,k}^\top)^\top$  and set  $\Delta_{j,0,k} = -\infty$ ,  $\Delta_{j,C_j,k} = \infty$ . This latent-threshold formulation is standard for ordinal responses (Muthén, 1984; Uebersax, 1999); special cases include Guo et al. (2015), which corresponds to  $K = 1$ , and Lee et al. (2022), which assumes class-homogeneous thresholds  $\boldsymbol{\Delta}_{j,k} \equiv \boldsymbol{\Delta}_j$ . When clear from context, we sometimes drop the individual-level index  $i$  and write  $Z, \mathbf{X}, \mathbf{R}$ .

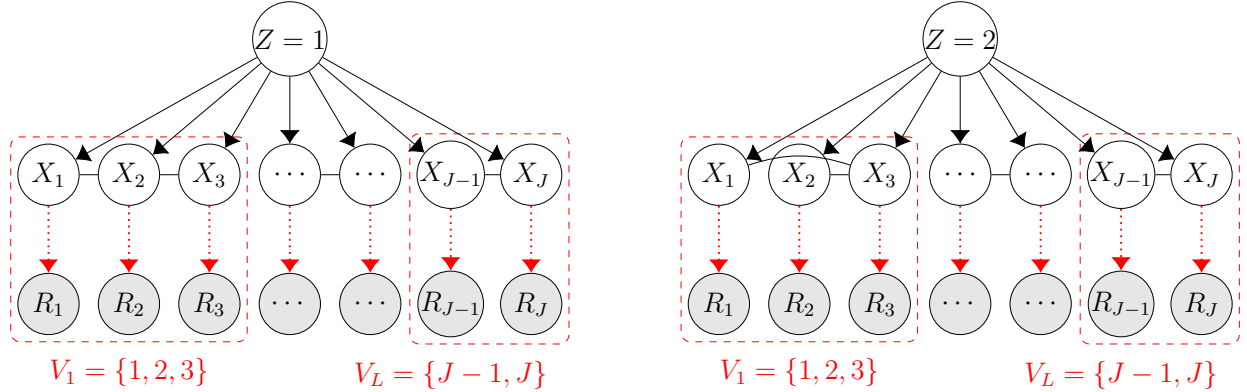


Figure 1: Graphical model illustration of the data generating process. Here,  $Z$  denotes the categorical latent class,  $\mathbf{X} = (X_1, \dots, X_J)^\top$  denotes the Gaussian latent vector, and  $\mathbf{R} = (R_1, \dots, R_J)^\top$  denotes the ordinal response vector. The dotted red boxes indicate the shared block structure, while the within-block graphical structure may vary across latent classes. We omit the individual-level index  $i$  for simplicity.

Our key modeling assumption is a *shared block dependence* structure across all  $K$  mixture components. To elaborate, assume that the  $J \times J$  covariance matrices  $\boldsymbol{\Sigma}_k = (\sigma_{(j,j'),k})_{j,j' \in [J]}$

are block-diagonal after appropriately permuting the row/column indices:

$$\Sigma_k = \begin{pmatrix} \Sigma_k^{(1)} & 0 & \cdots & 0 \\ 0 & \Sigma_k^{(2)} & \cdots & 0 \\ \vdots & \vdots & \ddots & \vdots \\ 0 & 0 & \cdots & \Sigma_k^{(L)} \end{pmatrix} = \text{diag}(\Sigma_k^{(1)}, \dots, \Sigma_k^{(L)}), \quad k = 1, \dots, K. \quad (5)$$

Here, each  $\Sigma_k^{(\ell)}$  is positive definite with size  $J_\ell \times J_\ell$ ,  $L$  is the number of blocks, and  $\sum_{\ell=1}^L J_\ell = J$ . For notational convenience, define a vertex set  $V = [J] = \cup_{\ell=1}^L V_\ell$ , so that each  $V_\ell$  denotes the vertices belonging to the  $\ell$ th block and  $|V_\ell| = J_\ell$ .

To ensure that the block structure is well-defined (in the sense that there is no finer possible partition of  $[J]$ ), we impose the following assumption.

**Assumption 1.** *For any  $\ell \in [L]$ , define a graph on  $V_\ell$  with edges  $E_\ell = \{(j, j') : j \neq j' \in V_\ell, \max_k |\sigma_{(j,j'),k}| > \epsilon_N\}$ , where  $\epsilon_N > 0$  is a quantity that is allowed to converge to 0 as  $N$  grows. Assume that the graph  $(V_\ell, E_\ell)$  is connected.*

The connectivity in Assumption 1 ensures local dependence within each block. In contrast, items in different blocks are constrained to be conditionally independent.

To further understand finer conditional dependence relationships within each block, it is helpful to introduce the precision matrices  $\Omega_k = \Sigma_k^{-1} = (\omega_{(j,j'),k})_{j,j' \in [J]}$ :

$$\Omega_k = \text{diag}(\Omega_k^{(1)}, \dots, \Omega_k^{(L)}), \quad k = 1, \dots, K.$$

Here, the block diagonal structure of  $\Omega_k$  follows immediately from that of  $\Sigma_k$  in (5). Since  $\mathbf{X} \mid (Z = k)$  follows a Gaussian graphical model with precision matrix  $\Omega_k$ , the usual conditional independence relationships follow: for  $j \neq j'$ ,  $\omega_{(j,j'),k} = 0$  if and only if  $X_j \perp\!\!\!\perp X_{j'} \mid (X_{[J] \setminus \{j,j'\}}, Z = k)$ . For notational convenience, denote the collections of all covariance and precision matrices as  $\Sigma = (\Sigma_1, \dots, \Sigma_K)$  and  $\Omega = (\Omega_1, \dots, \Omega_K)$ , respectively.

The classical locally independent LCM (see Section 2.1) is recovered by taking  $L = J$  and  $J_\ell = 1$  for each  $\ell \in [L]$ . The covariance matrices simply reduce to  $\Sigma_k^{(\ell)} = 1$ , and we recover the conditional independence of the responses. This is equivalent to directly parametrizing

the conditional response probabilities, e.g.  $\mathbb{P}(R_j = a \mid Z = k) = \theta_{j,a,k}$  as in (2).

## 2.3 Assumptions

We describe two general assumptions that will be imposed for all theoretical results. We first assume that the number of ordinal categories is bounded. This is a natural assumption in the context of our applications, such as surveys or ratings, for which the number of categories is fundamentally bounded.

**Assumption 2** (Bounded number of categories). *Assume that  $C_{\max} := \max_{j \in [J]} C_j < \infty$ .*

Next, we impose some assumptions regarding the parameter values.

**Assumption 3** (Bounded parameter space). *Assume that there exist constants  $\delta_1, \delta_2, \delta_3, M > 0$  such that, for every  $k \in [K]$  and every  $j \neq j' \in [J]$ ,*

$$|\sigma_{(j,j'),k}| \leq 1 - \delta_1, \quad \max_{a \in [C_j-1]} |\Delta_{j,a,k}| \leq M, \quad \min_{2 \leq a \leq C_j-1} |\Delta_{j,a,k} - \Delta_{j,a-1,k}| \geq \delta_2, \quad \pi_k \geq \frac{\delta_3}{K}.$$

Here, the first part regarding  $\Sigma_k$  rules out the degeneracy where two entries of the latent Gaussian  $\mathbf{X}$  are nearly collinear. The second and third parts require minimum separation between the thresholds  $\Delta_{j,a}$ , and ensure that the probability of each category is bounded away from zero. For the special case of binary observations with  $C_j = 2$ , the third condition can be ignored. Finally, the assumption on the proportion  $\boldsymbol{\pi}$  states that all  $K$  latent classes have comparable cluster sizes, and is included mainly for simpler presentation.

## 3 Estimation Method with Entry-wise Guarantees

Given the  $N \times J$  observation matrix  $\mathbf{R}$  generated from (1)–(4), our goal is to estimate the model components:

- (a) the latent-class vector  $\mathbf{Z} = (Z_1, \dots, Z_N)^\top$ ,
- (b) the number of blocks  $L$  and the partition of the vertices  $\{V_1, \dots, V_L\}$ ,
- (c) the covariance/precision matrices  $\boldsymbol{\Sigma}, \boldsymbol{\Omega}$ ,

(d) other continuous parameters (the latent class proportions  $\boldsymbol{\pi}$  and the thresholds  $\boldsymbol{\Delta}$ ).

For simplicity, we will assume that the number of latent classes  $K$  is known throughout this section (see Supplement D.3 for details on selecting  $K$ ).

As mentioned in the introduction, our estimation pipeline consists of three steps, which we outline below:

1. Recovering  $\mathbf{Z}, \boldsymbol{\pi}, \boldsymbol{\Delta}$  via spectral clustering (see Section 3.1),
2. Estimating the covariance matrices  $\boldsymbol{\Sigma}$  and the block structure by estimating pairwise polychoric correlations (see Section 3.2),
3. Estimating the precision matrices  $\boldsymbol{\Omega}$  and finer graphical structures (see Section 3.3).

In addition to describing the algorithm, each of the first three subsections below provides theoretical finite-sample error bounds, whose proofs are postponed to Supplement B. Further details regarding practical implementation choices are given in Section 3.4.

### 3.1 Step 1: Spectral clustering based on the flattened responses

Spectral clustering is a computationally efficient method widely used in network community detection and mixture models (Chen et al., 2021; Abbe et al., 2022; Zhang and Zhou, 2024). We leverage the approximate low-rank structure of the  $N \times J$  response matrix  $\mathbf{R}$  to recover the latent-class vector  $\mathbf{Z}$ . To see the motivation, first consider the special case where all responses are binary (i.e.,  $C_j = 2$  for all  $j$ ) and  $R_{i,j}$  takes values 0, 1. Then, (3)–(4) imply

$$\mathbb{E}[R_{i,j} \mid (Z_i = k)] = 1 - \Phi(\Delta_{j,1,k}) := \theta_{j,k}. \quad (6)$$

In matrix form, we can write  $\mathbb{E}[\mathbf{R} \mid \mathbf{Z}] = \mathbf{Y}\boldsymbol{\Theta}^\top$ , where  $\mathbf{Y}$  is the  $N \times K$  matrix whose  $i$ th row is a one-hot encoding vector of the corresponding scalar latent-class label  $Z_i \in [K]$ , and  $\boldsymbol{\Theta} = (\theta_{j,k})$  is a  $J \times K$  matrix storing the latent-class-specific conditional response probabilities. This shows that the data  $\mathbf{R}$  can be written as the sum of a low-rank matrix  $\mathbf{Y}\boldsymbol{\Theta}^\top$  with rank at most  $K$  and a mean-zero noise matrix  $\mathbf{R} - \mathbf{Y}\boldsymbol{\Theta}^\top$ .

In the context of mixture models, spectral clustering is mainly used for real-valued data.

In our general setup with potentially  $C_j > 2$ , one challenge arises from the ordinal nature of the responses. As the response space is non-Euclidean, it is unclear at first glance how to expose the approximate low-rank structure and use it for clustering. We therefore use the data-flattening technique of [Chen et al. \(2026\)](#) to transform the data into a *flattened binary matrix*, defining an  $N \times \sum_{j=1}^J C_j$  matrix  $\tilde{\mathbf{R}}$  by

$$\tilde{R}_{i, \sum_{m=1}^{j-1} C_m + a} = \mathbb{I}(R_{i,j} = a), \quad \text{for } a \in [C_j]. \quad (7)$$

In  $\tilde{\mathbf{R}}$ , each ordinal entry  $R_{i,j} \in [C_j]$  is replaced by a one-hot encoding vector of length  $C_j$ . For example, when  $C_j = 3$ ,  $R_{i,j} = 1$  is replaced by  $(1, 0, 0)$ , and  $R_{i,j} = 2$  is replaced by  $(0, 1, 0)$ .

After this transformation, the conditional expectation of the flattened data matrix  $\tilde{\mathbf{R}}$  can be spelled out similarly to (6):

$$\begin{aligned} \mathbb{E}[\tilde{R}_{i, \sum_{m=0}^{j-1} C_m + a} \mid (Z_i = k)] &= \mathbb{P}(R_{i,j} = a \mid (Z_i = k)) \\ &= \Phi(\Delta_{j,a,k}) - \Phi(\Delta_{j,a-1,k}) := \theta_{j,a,k}, \quad \forall j \in [J], a \in [C_j]. \end{aligned} \quad (8)$$

In matrix form,  $\mathbb{E}[\tilde{\mathbf{R}} \mid \mathbf{Z}] = \mathbf{Y}\Theta^\top$ , where  $\Theta$  is a  $(\sum_{j=1}^J C_j) \times K$  matrix. This low-rank expectation structure implies that spectral clustering can be applied to  $\tilde{\mathbf{R}}$ . The overall procedure is outlined in [Algorithm 1](#), where we mainly follow the implementation in [Zhang and Zhou \(2024\)](#).

Let  $\hat{\mathbf{Z}} \in [K]^N$  denote the estimated cluster labels (see (9)), and let  $\hat{N}_k = \sum_{i=1}^N \mathbb{I}(\hat{Z}_i = k)$  denote the estimated size of the  $k$ th cluster. To evaluate the clustering accuracy, define the misclustering error (Hamming loss) as:

$$\ell(\hat{\mathbf{Z}}, \mathbf{Z}) := \min_{S \in \mathcal{S}_{[K]}} \sum_{i=1}^N \mathbb{I}(\hat{Z}_i \neq S(Z_i)). \quad (10)$$

Here, the minimum taken over permutations  $\mathcal{S}_{[K]}$  is necessary due to label permutation. Define  $\tilde{J}_{\max}$  as the maximum length of a flattened block in  $\tilde{\mathbf{R}}$ , and  $D$  as the minimum

---

**Algorithm 1:** Spectral Clustering of Polytomous LCMs based on Flattening

---

**Input:** Data matrix  $\mathbf{R} = (\mathbf{R}_1^\top, \dots, \mathbf{R}_N^\top)^\top \in \mathbb{R}^{N \times J}$ , number of clusters  $K$

**Output:** Cluster assignment vector  $\hat{\mathbf{Z}} \in [K]^N$

- 1 Flatten the  $N \times J$  ordinal matrix  $\mathbf{R}$  into a  $N \times \sum_{j=1}^J C_j$  binary matrix  $\tilde{\mathbf{R}}$  as in (7).
- 2 Compute a top- $K$  SVD of  $\tilde{\mathbf{R}}$ :

$$\tilde{\mathbf{R}} \approx \hat{\mathbf{U}} \hat{\mathbf{\Lambda}} \hat{\mathbf{W}}^\top = \sum_{i=1}^K \hat{\sigma}_i \hat{\mathbf{u}}_i \hat{\mathbf{w}}_i^\top,$$

where  $\hat{\sigma}_1 \geq \hat{\sigma}_2 \geq \dots \geq \hat{\sigma}_K \geq 0$  and  $\{\hat{\mathbf{u}}_i\}_{i=1}^K \in \mathbb{R}^N$ ,  $\{\hat{\mathbf{w}}_i\}_{i=1}^K \in \mathbb{R}^{\sum_{j=1}^J C_j}$ .

- 3 Perform  $k$ -means clustering on the rows of  $\tilde{\mathbf{R}} \hat{\mathbf{W}} = \hat{\mathbf{U}} \hat{\mathbf{\Lambda}}$ :

$$\left\{ \hat{\mathbf{z}}, \{\hat{\mathbf{d}}_k\}_{k \in [K]} \right\} = \underset{\mathbf{z} \in [K]^N, \{\mathbf{d}_k\}_{k \in [K]}}{\operatorname{argmin}} \sum_{i \in [N]} \|\hat{\mathbf{W}}^\top \tilde{\mathbf{R}}_i - \mathbf{d}_{z_i}\|^2. \quad (9)$$


---

separation between the threshold vectors  $\Delta_k$ :

$$\tilde{J}_{\max} := \max_{\ell=1}^L \sum_{j \in V_\ell} C_j, \quad D := \min_{k \neq k' \in [K]} \|\Delta_k - \Delta_{k'}\|.$$

The following proposition provides exact recovery guarantees for the latent-class vector  $\mathbf{Z}$  in the high-dimensional regime. Note that all dimensions  $N, J, \tilde{J}_{\max}, K$  are allowed to grow, while  $\tilde{J}_{\max}$  and  $K$  may also be of constant order.

**Proposition 1.** *Suppose that Assumptions 2, 3 hold. There exist constants  $c_1, c_2 > 0$  (that depend on  $C_{\max}, \delta_3, M$ ) such that when  $\min(D, \sqrt{K} \sigma_K(\Theta)) \geq c_1 K \sqrt{\tilde{J}_{\max}} (1 + \sqrt{J/N})$  and  $c_1 N \geq K^2$ , we have*

$$\mathbb{E} \ell(\hat{\mathbf{Z}}, \mathbf{Z}) \leq N \left( e^{-c_2 D^2 / \tilde{J}_{\max}} + K e^{-c_2 N / K} \right) =: p_1. \quad (11)$$

*In particular, when  $D \geq c_3 \sqrt{\tilde{J}_{\max} \log N}$  for some large enough  $c_3 > 0$ , the right hand side of (11) is  $O(N^{-1})$ , so  $\hat{\mathbf{Z}}$  achieves **exact recovery** with probability at least  $1 - O(N^{-1})$ .*

We discuss the conditions required in Proposition 1. First, the lower bound for  $D$  requires all cluster means to be sufficiently separated. Note from (8) that the thresholds  $\Delta_k$  (which are used to define  $D$ ) are directly related to the cluster centers  $\theta_k$ . Second, the lower bound

for  $\sigma_K(\Theta)$  requires a sufficiently large spectral gap, and is a standard requirement for the success of spectral methods. The condition  $N \gtrsim K^2$  is a mild technical requirement that arises from [Zhang and Zhou \(2024\)](#).

The following simplified scaling discussion is provided only for illustration and interpretation; the additional conditions imposed in this paragraph are not required for the conclusion of Proposition 1 to hold. To further understand the scaling requirement, suppose  $K = O(1)$ . Also, assume homogeneous block sizes and response categories (i.e.,  $J_1 = \dots = J_L \equiv J/L, C_1 = \dots = C_J \equiv C$ ), so that  $\tilde{J}_{\max} = O(J/L)$ . As  $\Delta_k$  is an  $O(J)$ -dimensional parameter, we can view  $D$  as  $O(\sqrt{J})$  when the latent classes are distinct across all items. Then, the requirement for  $D$  simplifies to assuming a *growing number of blocks* so that  $L \gtrsim \log N + J/N$ . Taking  $\sigma_K(\Theta) \asymp \sqrt{J}$ , the requirement for  $\sigma_K(\Theta)$  also reduces to  $L \gtrsim 1 + J/N$ . Note that these requirements are relatively mild and allow both  $J > N$  as well as  $N > J$ . In general, the requirement for  $L$  becomes more stringent when different latent classes are less separated or the number of clusters  $K$  increases.

Now, given the estimated cluster labels, it is straightforward to estimate the mixture proportion vector  $\pi$  as well as the threshold vector  $\Delta$ . To simplify notation, assume without loss of generality that the estimated labels are correctly permuted in the sense that  $\hat{Z}_i = Z_i$ . The latent class proportions can be estimated based on the latent class labels,  $\hat{\pi}_k := \hat{N}_k/N$ . Recalling (4), the conditional probability of observing a response of  $a$  or lower is  $\mathbb{P}(R_j \leq a \mid Z = k) = \Phi(\Delta_{j,a,k})$ . A natural moment estimator arises by replacing the left hand side  $\mathbb{P}(R_j \leq a \mid Z = k)$  of this population identity with the empirical probability conditional on the  $k$ th latent class:

$$\hat{\Delta}_{j,a,k} := \Phi^{-1} \left( \frac{1}{\hat{N}_k} \sum_{i: \hat{Z}_i = k} \mathbb{I}(R_{i,j} \leq a) \right), \quad \forall a \in [C_j - 1].$$

This estimator can also be obtained from the estimated  $K$ -dimensional centers  $\hat{d}_k$  in (9) by mapping them back to the original  $J$ -dimensional scale and writing out the k-means criterion; see eq. (15) in [Zhang and Zhou \(2024\)](#) for further details.

The following proposition gives entry-wise estimation error bounds for both  $\hat{\pi}$  and  $\hat{\Delta}$ .

**Proposition 2.** *Assuming all conditions in Proposition 1, there exist constants  $c_1, c_2 = c_2(M, \delta_3) > 0$  such that*

$$\mathbb{P}\left(\max_{k \in [K]} |\hat{\pi}_k - \pi_k| \geq t\right) \leq Ke^{-c_1 N t^2} + O(N^{-1}),$$

$$\mathbb{P}\left(\max_{k \in [K]} \max_{j \in [J], a \in [C_j - 1]} |\hat{\Delta}_{j,a,k} - \Delta_{j,a,k}| \geq t\right) \leq \left(\sum_{j=1}^J C_j\right) Ke^{-c_2 N t^2 / K} + O(N^{-1}),$$

for all  $0 < t < M$ .

In particular, both estimators for  $\boldsymbol{\pi}$  and  $\boldsymbol{\Delta}$  are  $\sqrt{N}$ -consistent, up to the log factors in  $K, J$  that arise from a uniform bound. This result suggests that the proposed spectral clustering method based on the flattened data matrix delivers an entrywise consistent estimator for the latent class proportions and the threshold values for the ordinal variables, laying the foundation for subsequent steps.

## 3.2 Step 2: Estimating covariance matrix and block structures

Our second step aims to recover the block dependence structure by partitioning the set of vertices  $V = [J]$  into disjoint sets  $V_1, \dots, V_L$ . The key idea is to separately estimate the class-specific latent covariance matrices  $\boldsymbol{\Sigma}_k$  for each latent class  $k$ , and aggregate their sparsity patterns to estimate the partition shared across latent classes.

We first consider estimating the covariance matrices  $\boldsymbol{\Sigma}_k$  for each cluster. If the latent Gaussian variables  $X_{i,j}$  were observed, one could simply use the sample covariance matrix. However, with ordinal responses, this is not feasible. A naive solution would be to compute the MLE of  $\boldsymbol{\Sigma}_k$  given the responses within the  $k$ th cluster. However, computing this is challenging as  $\boldsymbol{\Sigma}_k$  has  $O(J^2)$  entries and is required to be positive definite.

Therefore, we relax the positive definite constraint and estimate each off-diagonal entry separately. Our key observation is that  $\sigma_{(j,j'),k}$  is exactly the *polychoric correlation* between observations  $R_j$  and  $R_{j'}$ , conditioned on the latent class  $k$ . To the statistical audience, the terminology “tetrachoric correlation” (Pearson, 1900) may be more familiar, which is a special case of the polychoric correlation when both  $R_j$  and  $R_{j'}$  are binary. Estimating pairwise

polychoric correlation from ordinal responses has been a classical topic in psychometrics and categorical data analysis (Lancaster and Hamdan, 1964; Olsson, 1979; Muthén, 1984; Bonett and Price, 2005). Motivated by Olsson (1979), we focus on the following pseudo-MLE that maximizes the likelihood of  $(R_j, R_{j'})$  while treating the threshold vector  $\Delta_k$  as fixed:

$$\begin{aligned} \hat{\sigma}_{(j,j'),k} &:= \operatorname{argmax}_{|\sigma| \leq 1 - \delta_1} \sum_{i: \hat{Z}_i = k} \log \mathbb{P}(R_j^{(\sigma)} = R_{i,j}, R_{j'}^{(\sigma)} = R_{i,j'} \mid Z = k; \hat{\Delta}_k) \\ &= \operatorname{argmax}_{|\sigma| \leq 1 - \delta_1} \sum_{i: \hat{Z}_i = k} \log \mathbb{P}\left(X_j^{(\sigma)} \in [\hat{\Delta}_{j,R_{i,j}-1,k}, \hat{\Delta}_{j,R_{i,j},k}), X_{j'}^{(\sigma)} \in [\hat{\Delta}_{j',R_{i,j'}-1,k}, \hat{\Delta}_{j',R_{i,j'},k})\right). \end{aligned} \quad (12)$$

Here,  $(X_j^{(\sigma)}, X_{j'}^{(\sigma)})$  is the latent Gaussian vector, distributed as a bivariate standard normal with correlation  $\sigma$ . Also,  $R_j^{(\sigma)}$  denotes the random variable discretized from  $X_j^{(\sigma)}$  via (4), and  $R_{i,j}$  is the observation from the  $i$ th individual.

**Remark 1** (Connection to rank-based estimators in semiparametric statistics). *There are alternative estimators in the ordinal Gaussian copula literature that estimate pairwise latent correlations by inverting Kendall's-tau moment equations: Fan et al. (2017) considers the binary responses case, and Feng and Ning (2019) and Quan et al. (2018) consider the ordinal case. When all variables are binary, (12) is essentially equivalent to the Kendall's tau estimator. This equivalence no longer holds when at least one response has  $C_j > 2$  categories, which is why Feng and Ning (2019) considered an ensemble estimator that aggregates estimates based on binarized responses and Quan et al. (2018) limits to ternary data (with  $C_j = 3$ ), both of which result in information loss for general ordinal data. In contrast, the likelihood-based estimator (12) we employ uses the full  $C_j \times C_{j'}$  contingency table to estimate the correlation and allows arbitrary numbers of categories per variable.*

**Remark 2** (Fixing the threshold estimates). *The careful reader may have noticed that the threshold vectors  $\Delta_k$  are treated as constants in the likelihood (12). This is because  $\Delta_k$  are already estimated consistently in Step 1, and because joint maximum likelihood over  $(\Delta_k, \Sigma_k)$  is computationally prohibitive even for moderate  $J$  (Olsson, 1979; Welz et al., 2026). Without fixing  $\Delta_k$ , pairwise estimation is no longer possible, since each  $\Delta_{j,k}$  appears in the likelihood for all  $\{\sigma_{(j,j'),k} : j' \neq j\}$ . A similar strategy was used in the works cited in Remark 1.*

Now, we can ensure that each entry of the covariance matrices  $\Sigma_k$  is accurately estimated, at a  $\sqrt{N/K}$  rate. Here,  $N/K$  is the effective within-class sample size, due to Assumption 3. In fact, taking  $K = 1$ , the resulting rate (including the log factor) matches the usual estimation error rate for Gaussian graphical models and semiparametric copulas (Liu et al., 2012), despite observing only discrete data. The proof of Proposition 3 builds upon an exponential concentration inequality for the pairwise polychoric correlation estimator (12), which may be of independent interest (see Lemma 1 in the Supplementary Material).

**Proposition 3.** *Consider the setting of Proposition 1. For any  $t > 0$ , there exist constants  $c_1, c_2, c_3 > 0$  (that depend on  $C_{\max}, \delta_1, \delta_2, \delta_3, M$ ) such that the following holds:*

$$\mathbb{P}\left(\max_{k=1}^K \|\widehat{\Sigma}_k - \Sigma_k\|_{\max} \geq t\right) \leq c_1 K J^2 \left(e^{-c_2 N t^2 / K} + e^{-c_3 N / K}\right) + p_1. \quad (13)$$

Hence, there exists another constant  $c_4 > 0$  such that  $\max_{k=1}^K \|\widehat{\Sigma}_k - \Sigma_k\|_{\max} \leq \tau_1 := c_4 \sqrt{K \log(JK) / N}$  with probability greater than  $1 - O((JK)^{-1} + N^{-1})$  provided that  $N \gtrsim K \log(JK)$ .

Consequently, we can also learn the global block structure among  $X_1, \dots, X_J$ , i.e., estimate  $\widehat{L}$  and the partition  $V = [J] = \cup_{\ell=1}^{\widehat{L}} \widehat{V}_\ell$ . Our main idea is to aggregate the sparsity information across all latent classes, as a single latent class may potentially exhibit additional sparsity and therefore a finer block structure than the shared global block structure. See the top row in Figure 2 for a visualization of  $\Sigma_1$  and  $\widehat{\Sigma}_1$ , where the block structure is not evident from  $\widehat{\Sigma}_1$  alone. To this end, we define a  $J \times J$  binary matrix  $\mathbf{G}$  by setting each entry as  $g_{(j,j')}$  :=  $\mathbb{I}(\max_{k=1}^K |\widehat{\sigma}_{(j,j'),k}| > \tau_1)$ , and view it as an adjacency matrix on the set of nodes  $V$ . By Proposition 3,  $\mathbf{G}$  includes the edges  $\cup_{\ell=1}^{\widehat{L}} E_\ell$ , where  $E_\ell$  is as in Assumption 1. Then, we can read off the block structure from  $\mathbf{G}$  by setting  $\widehat{L}$  as the number of connected components, and letting  $\widehat{V}_1, \dots, \widehat{V}_{\widehat{L}}$  be vertices in each connected component. The following proposition establishes consistency of this estimator.

**Proposition 4.** *Continuing from Proposition 3, additionally suppose that the constant  $\epsilon_N$  in Assumption 1 satisfies  $\epsilon_N \geq 2\tau_1$ . Then,  $\widehat{L} = L$  and  $\{\widehat{V}_1, \dots, \widehat{V}_{\widehat{L}}\} = \{V_1, \dots, V_L\}$  with*

probability greater than  $1 - O((JK)^{-1} + N^{-1})$ .

Given this result, we can now fix the global block structure. For notational convenience and without loss of generality, on the event that  $V$  is correctly partitioned, assume that the learned blocks are indexed correctly; i.e.,  $\widehat{V}_\ell = V_\ell$  for all  $\ell$ .

### 3.3 Step 3: Learning precision matrix and within-block structures

Having estimated the “global” block structure shared by all latent classes, we now consider the problem of estimating the “local” sparsity structure encoded in each precision matrix  $\Omega_k^{(\ell)}$  for each block  $\ell$  and each latent class  $k$ . Note that imposing the block structure greatly reduces the dimension of the precision matrices from  $J(J+1)/2$  to  $\sum_{\ell=1}^L J_\ell(J_\ell+1)/2$ . Since no common structure is imposed within blocks, each  $\Omega_k^{(\ell)}$  is separately estimated.

Here, the main idea is to use sparse precision matrix estimators from their covariance matrix counterparts  $\Sigma_k^{(\ell)}$ . For this purpose, for any  $k \in [K], \ell \in [L]$ , one can use the usual graphical lasso estimator (Friedman et al., 2008; Yuan and Lin, 2007, among others):

$$\widehat{\Omega}_k^{(\ell)} = \underset{\Omega_k^{(\ell)} \in \mathbb{R}^{|\widehat{V}_\ell| \times |\widehat{V}_\ell|}}{\operatorname{argmax}} \log |\Omega_k^{(\ell)}| - \operatorname{tr}(\widehat{\Sigma}_k^{(\ell)} \Omega_k^{(\ell)}) - \lambda \sum_{j \neq j' \in \widehat{V}_\ell} |\omega_{(j,j'),k}^{(\ell)}|,$$

or the CLIME estimator (Cai et al., 2011):

$$\widetilde{\Omega}_k^{(\ell)} = \underset{\Omega_k^{(\ell)} \in \mathbb{R}^{|\widehat{V}_\ell| \times |\widehat{V}_\ell|}}{\operatorname{argmin}} \|\Omega_k^{(\ell)}\|_1 \quad \text{s.t.} \quad \|\widehat{\Sigma}_k^{(\ell)} \Omega_k^{(\ell)} - \mathbf{I}\|_{\max} \leq \lambda, \quad (14)$$

$$\widehat{\omega}_{(j,j'),k} = \widehat{\omega}_{(j',j),k} := \begin{cases} \widetilde{\omega}_{(j,j'),k}, & \text{if } |\widetilde{\omega}_{(j,j'),k}| \leq |\widetilde{\omega}_{(j',j),k}|, \\ \widetilde{\omega}_{(j',j),k}, & \text{otherwise,} \end{cases} \quad \forall j, j' \in [J]. \quad (15)$$

Here, the initial estimator in (14) may be asymmetric, so this is symmetrized in (15) by taking the entry with smaller magnitude.

For a simpler presentation, here we focus on analyzing the CLIME estimator (15). For this purpose, we require additional assumptions on the true precision matrix.

**Assumption 4** (Precision matrix assumptions). (a) For each  $k \in [K], \ell \in [L]$ , suppose that  $\mathbf{\Omega}_k^{(\ell)}$  satisfies  $\|\mathbf{\Omega}_k^{(\ell)}\|_1 \leq M'_N$  for some  $M'_N > 0$ .

(b) Additionally, for some constant  $\epsilon'_N > 0$ , assume a minimal signal strength condition

$$\min_{j, j' \in V_\ell: \omega_{(j, j'), k}^{(\ell)} \neq 0} |\omega_{(j, j'), k}^{(\ell)}| > \epsilon'_N.$$

Assumption 4 is a standard requirement in Cai et al. (2011) that helps theoretically understand the CLIME estimator. Part (b) in Assumption 4 requires a minimal signal strength for the nonzero precision matrix entries as opposed to the analogous condition for selecting covariance matrix entries in Assumption 1.

Now, we state our main theoretical result on precision matrix estimation. Again, the resulting bounds are of the same order as those for Gaussian graphical models.

**Proposition 5.** Consider the setting in Proposition 4 and suppose Assumption 4(a) holds. Consider the precision matrix estimate  $\widehat{\mathbf{\Omega}}_k^{(\ell)}$  in (15) with  $\lambda = M'_N \tau_1$ .

(a) With probability  $1 - O((JK)^{-1} + N^{-1})$ , we have

$$\|\widehat{\mathbf{\Omega}}_k^{(\ell)} - \mathbf{\Omega}_k^{(\ell)}\|_{\max} \leq 4M'_N \lambda.$$

(b) Additionally, let Assumption 4(b) hold for some  $\epsilon'_N \geq 8M'_N \lambda$ . Then, for  $\tau_2 = 4M'_N \lambda$ , the thresholded estimator  $\widetilde{\mathbf{\Omega}}_k^{(\ell)}$  with

$$\widetilde{\omega}_{(j, j'), k}^{(\ell)} := \widehat{\omega}_{(j, j'), k}^{(\ell)} \mathbb{I}(|\widehat{\omega}_{(j, j'), k}^{(\ell)}| \geq \tau_2)$$

is sign consistent, i.e.,  $\text{sgn}(\widetilde{\omega}_{(j, j'), k}^{(\ell)}) = \text{sgn}(\omega_{(j, j'), k}^{(\ell)})$  with probability  $1 - O((JK)^{-1} + N^{-1})$ .

**Remark 3.** Similar sign-consistency guarantees can potentially be derived for other sparsity-inducing procedures, such as the graphical lasso, by applying the so-called “meta-theorem” (cf. Thm 4.3 in Liu et al. (2012)) to the entry-wise guarantees for  $\mathbf{\Sigma}_k$  in Proposition 3. To this end, one would need to replace Assumption 4 with the usual Lasso assumptions, such as mutual incoherence.

Finally, we combine all results in Propositions 1–5 to obtain the following theorem.

**Theorem 1.** *Under the conditions of Propositions 1–5, which include the scaling requirement  $N \gtrsim K^2 + K \log(JK)$ , all model components (a)–(d) can be consistently estimated.*

Thus, our three-step estimation procedure provides end-to-end consistency for estimating all model components in the block-dependent latent class model.

### 3.4 Additional choices for implementation

**Learning the block structures** While the binary matrix  $\mathbf{G}$  (see the text just before Proposition 4) suffices for theoretical purposes, it can lead to false discovery under limited sample sizes (i.e., some zero values in the off-block-diagonals are estimated as one). Such errors can blur the connectivity structure between the blocks, as illustrated in the left panel in the second row of Figure 2.

To provide a more robust and practical solution for learning the shared block structure, we propose using network community detection on a continuous aggregation matrix. Specifically, we aggregate the *magnitudes* of the estimated polychoric correlations (as opposed to the binary matrix  $\mathbf{G}$ ) and define a  $J \times J$  weighted adjacency matrix  $\tilde{\mathbf{G}}$  with zero diagonals:

$$\tilde{g}_{j,j'} := \begin{cases} \frac{1}{K} \sum_{k=1}^K |\hat{\sigma}_{(j,j'),k}| \mathbb{I}(|\hat{\sigma}_{(j,j'),k}| \geq \tau_1) & \text{if } j \neq j', \\ 0 & \text{if } j = j'. \end{cases} \quad (16)$$

Here,  $\tilde{\mathbf{G}}$  can be made tuning-free by not thresholding the estimates  $\hat{\sigma}_{(j,j'),k}$ . Treating  $\tilde{\mathbf{G}}$  as a weighted adjacency matrix on  $V = [J]$ , we can estimate the shared block structure by generic graph community detection. This is because the off-block-diagonal entries are mostly small by Proposition 3, while within-block entries form connected components.

For community detection, we use the Leiden algorithm (Traag et al., 2019) because it can estimate  $L$  and is well-suited for weighted graphs. In the center/right panel of the second row in Figure 2, Leiden accurately recovers the blocks under both versions of  $\tilde{\mathbf{G}}$ . This choice can be flexibly substituted with other methods, such as the Louvain algorithm (Blondel et al., 2008) or spectral clustering. The full procedure is summarized in Algorithm 2.

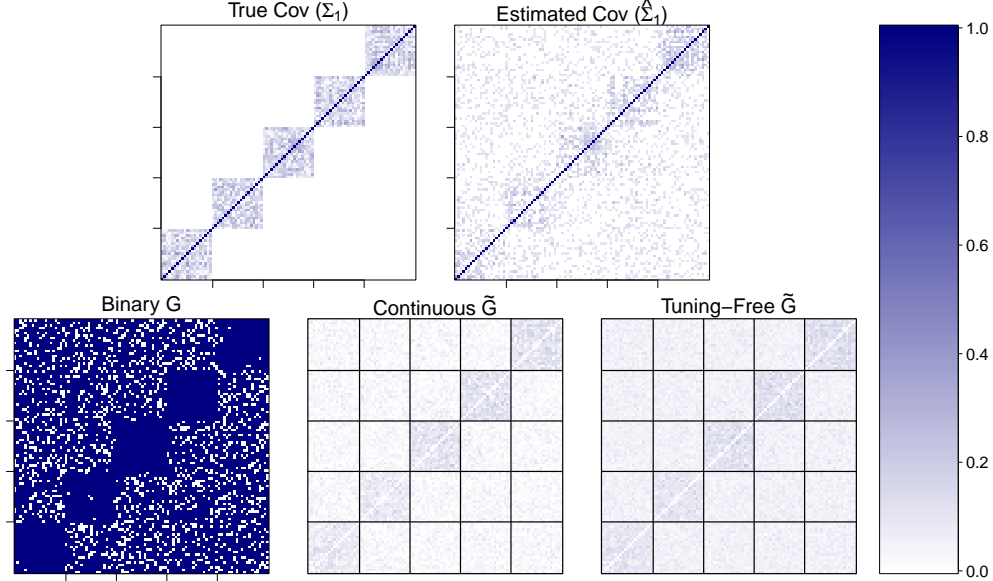


Figure 2: Covariance matrices and block-recovery for a simulated dataset (under the setting of the first row in Table 1). Top:  $|\Sigma_1|$  (left) and  $|\hat{\Sigma}_1|$  (right). Bottom: aggregation matrices for block structure recovery; the binary matrix  $\mathbf{G}$  (left), the continuous matrix  $\tilde{\mathbf{G}}$  (16) (center), and the tuning-free version of  $\tilde{\mathbf{G}}$  (right). Black lines mark the estimated blocks. The continuous matrices better capture the block signal despite the off-block noise.

---

**Algorithm 2:** Learning the shared block structure

---

**Input:** Estimated covariance matrices  $\{\hat{\Sigma}_k\}_{k \in [K]}$

**Output:** Estimated number of blocks  $\hat{L}$  and a partition  $\{\hat{V}_\ell\}_{\ell \in [\hat{L}]}$  of the variables  $[J]$

- 1 Construct the continuous weighted adjacency matrix  $\tilde{\mathbf{G}}$  as defined in (16).
  - 2 Apply a community detection algorithm (e.g., the Leiden algorithm) on  $\tilde{\mathbf{G}}$ .
  - 3 Let  $\hat{L}$  be the automatically detected number of communities, and let  $\{\hat{V}_\ell\}_{\ell \in [\hat{L}]}$  be the corresponding partition of the variables.
- 

The Leiden algorithm also has a *resolution parameter* that controls the granularity of the clustering, where a higher value produces a finer-grained partition with more clusters. In simulations, we use the default resolution parameter. In the real data analysis, we also consider a higher resolution parameter to find finer-grained blocks.

**Selecting the tuning parameter  $\lambda$**  The tuning parameter  $\lambda$  in (14) controls the level of sparsity in the estimated precision matrix. To select an optimal  $\lambda$ , we employ 5-fold cross-validation, a standard choice for sparse Gaussian graphical models (Rothman et al., 2008).

Information criteria such as BIC or EBIC (Chen and Chen, 2008; Barber and Drton, 2010) are alternatives, but in our experiments they tended to select overly sparse models when  $J$  was large, say above 100.

Note that one may further fine-tune  $\lambda$  for each cluster/block, by considering individual penalties  $\lambda_k^{(\ell)}$  for each  $\Omega_k^{(\ell)}$ . This could allow varying levels of sparsity across clusters/blocks.

## 4 Simulation Studies

We empirically assess the proposed method under the following simulation settings:

- **Dimensions:** We consider a fixed sample size  $N = 1000$  and vary (i) the number of variables  $J \in \{100, 500\}$ , (ii) the number of true blocks  $L \in \{5, 10\}$ , and (iii) the number of latent classes  $K \in \{5, 10\}$ .
- **Number of categories:** The first half of the  $J$  items are binary responses (i.e.,  $C_j = 2$ ), and the second half are four-category ordinal responses (i.e.,  $C_j = 4$ ).
- **Graph structure:** We consider two block-diagonal graph structures with varying sparsity of (iv)  $s = 0.2$  and  $s = 0.6$ . The graph within each block follows the Erdős-Rényi random graph with probability  $s$ , i.e., each off-diagonal entry within a block is non-zero with probability  $s$  and 0 with probability  $1 - s$ .

Data generation details are provided in Supplement D.1. Note that the range of  $J$  is high-dimensional in graphical modeling, as estimating  $\Omega = (\Omega_1, \dots, \Omega_K)$  entails  $KJ^2$  entries. For each setting, we run 100 replications and report the following averaged metrics:

- For the latent class assignments, we report (i)  $\text{Err}(\hat{\mathbf{Z}})$ , the misclustering error in (10).
- For the block recovery, we report (ii)  $\text{Err}(\hat{L}) = \mathbb{I}(\hat{L} \neq L)$ , i.e. the 0-1 loss for the estimated number of blocks. We also report the Adjusted Rand Index (ARI) (Hubert and Arabie, 1985) between the partitions  $\{V_1, \dots, V_L\}$  and  $\{\hat{V}_1, \dots, \hat{V}_{\hat{L}}\}$ , and denote it as (iii)  $\text{ARI}(\hat{V})$ . The value of 1 indicates perfect clustering and a near-zero value indicates uninformative (random) clustering.
- For the precision matrices  $\Omega$ , we report the (iv) support recovery (sparsity) error and

(v) Frobenius error:

$$\text{Err}_0(\widehat{\Omega}) := \frac{1}{KJ^2} \sum_{k=1}^K \sum_{j,j'=1}^J \mathbb{I}\left(\text{sgn}(\widehat{\omega}_{(j,j'),k}) \neq \text{sgn}(\omega_{(j,j'),k})\right),$$

$$\text{Err}_F(\widehat{\Omega}) := \frac{1}{\sqrt{KJ^2}} \sqrt{\sum_{k=1}^K \|\widehat{\Omega}_k - \Omega_k\|_F^2}.$$

$J$	$K$	$L$	$s$	$\text{Err}(\widehat{\mathbf{Z}})$	$\text{Err}(\widehat{L})$	1-ARI( $\widehat{V}$ )	$\text{Err}_0(\widehat{\Omega})$	$\text{Err}_F(\widehat{\Omega})$	time (s)
100	5	5	0.6	0.00	0.00	0.00	0.084	0.103	2.4
			0.2	0.00	0.00	0.00	0.085	0.099	2.3
		10	0.6	0.00	0.18	0.02	0.035	0.086	2.5
			0.2	0.00	0.41	0.06	0.038	0.084	2.3
	10	5	0.6	0.05	0.00	0.00	0.090	0.113	4.1
			0.2	0.06	0.00	0.00	0.068	0.113	3.9
		10	0.6	0.02	0.57	0.08	0.045	0.097	4.1
			0.2	0.04	0.67	0.09	0.038	0.097	4.1
500	5	5	0.6	0.00	0.00	0.00	0.102	0.060	47.0
			0.2	0.00	0.00	0.00	0.087	0.059	46.5
		10	0.6	0.00	0.00	0.01	0.052	0.058	46.5
			0.2	0.00	0.00	0.00	0.027	0.056	46.2
	10	5	0.6	0.00	0.00	0.00	0.106	0.067	83.7
			0.2	0.00	0.00	0.00	0.098	0.062	85.7
		10	0.6	0.00	0.02	0.00	0.051	0.058	83.2
			0.2	0.00	0.00	0.00	0.033	0.058	84.3

Table 1: Simulation results under varying dimensions  $J, K, L$  and sparsity  $s$ . The metrics are averaged over 100 replications, where the first column takes values in  $[0, N]$  with  $N = 1000$ , the second–fourth column takes values in  $[0, 1]$ , and the fifth column (the scaled Frobenius norm) is unbounded. For all columns, **smaller values are better**.

Table 1 illustrates that the proposed method consistently achieves high accuracy in all of clustering, block-structure recovery, and precision matrix estimation. Regarding clustering, exact clustering is possible except when  $J = 100, K = 10$ , and the clustering error is small even in this challenging setting. This aligns with theoretical insights from Proposition 1 that clustering is harder when  $J$  decreases and  $K$  increases. In Supplement E.1, we additionally discuss a one-step likelihood refinement procedure to further improve clustering accuracy.

Next, for block structure recovery, our method successfully identifies the true number of

blocks ( $\widehat{L} = L$ ) and achieves a high ARI for the estimated partition  $\{\widehat{V}_1, \dots, \widehat{V}_{\widehat{L}}\}$  in most of settings. Even when the point estimate  $\widehat{L}$  is incorrect, the high ARI (greater than 0.9) indicates that the resulting partitions are near-correct and informative; see Supplement E.3 for a visualization. We also observe that when  $\widehat{L}$  is incorrect, it is typically underestimated, i.e.,  $\widehat{L} \leq L$ . This may be an inherent limitation of modularity-based graph clustering algorithms when the block sizes  $J/L$  are small (Fortunato and Barthelemy, 2007; Traag et al., 2015), and we believe that this issue may be mitigated by fine-tuning the resolution parameter. See Supplement E.4 for further illustration regarding the resolution parameter.

Given the near-perfect recovery of the blocks, the precision matrices  $\Omega$  are also well estimated in terms of both the support and values. Overall, all reported accuracy measures are comparable as the sparsity level  $s$  changes, illustrating that our pipeline can handle unknown, varying sparsity. We will further discuss precision matrix estimation in the context of the comparison studies that will follow. Finally, the runtime reported in the last column of Table 1 demonstrates the scalability of the method.

**Comparison and ablation studies** We compare Steps 2–3 of our pipeline with the joint graphical lasso (JGL) from Danaher et al. (2014). After Step 1 and estimating the covariance matrices  $\widehat{\Sigma}_k$  in Step 2, JGL is a natural alternative because its joint penalty (across all  $k$ ) helps learn a common block-diagonal structure for the precision matrices, followed by within-block estimation. In fact, Danaher et al. (2014) proposed an explicit criterion that helps characterize block-diagonal structures and used it to scale up computation. We fix  $J = 100$  and use group JGL, which encourages shared sparsity across all  $K$  precision matrices.

Table 2 shows that the proposed method more accurately recovers the block structure and estimates the precision matrices. The ‘JGL-O’ column fixes  $\lambda_2 = 0.001$  and chooses  $\lambda_1$  from a grid with increment 0.001 so that the average  $\widehat{L}$  best matches the true number of blocks  $L$ , which is unavailable in practice. Even with this oracle-style tuning, JGL results in inconsistent block recovery in all settings. Also, JGL-CV always selects  $\widehat{L} = 1$  (no blocks detected), which indicates the need for careful tuning (see Supplement E.4 for additional

$K$	$L$	$s$	$\text{Err}(\widehat{L})$			$1\text{-ARI}(\widehat{V})$			$\text{Err}_F(\widehat{\Omega})$			time (s)		
			Ours	JGL-O	JGL-CV	Ours	JGL-O	JGL-CV	Ours	JGL-O	JGL-CV	Ours	JGL-O	JGL-CV
5	5	0.6	0.00	0.80	1.00	0.00	0.88	1.00	0.103	0.126	0.121	0.1	0.6	0.5
		0.2	0.00	0.70	1.00	0.00	0.36	1.00	0.099	0.133	0.124	0.1	0.5	0.4
	10	0.6	0.18	0.89	1.00	0.02	0.65	1.00	0.086	0.111	0.105	0.1	0.6	0.4
		0.2	0.41	0.74	1.00	0.06	0.21	1.00	0.084	0.116	0.108	0.1	0.5	0.4
10	5	0.6	0.00	0.84	1.00	0.00	1.00	1.00	0.113	0.132	0.132	0.1	1.1	0.9
		0.2	0.00	0.87	1.00	0.00	0.86	1.00	0.113	0.141	0.140	0.1	1.0	0.9
	10	0.6	0.57	0.89	1.00	0.08	0.96	1.00	0.097	0.117	0.117	0.1	1.2	0.9
		0.2	0.67	0.91	1.00	0.09	0.55	1.00	0.097	0.125	0.124	0.1	0.9	1.0

Table 2: Simulation results for  $J = 100$  while varying  $K, L, s$ . ‘Ours’ denotes the proposed method, and ‘JGL-O’/‘JGL-CV’ denotes the joint graphical lasso from [Danaher et al. \(2014\)](#), where the tuning parameter is fine-tuned using the true  $L$  in an oracle manner, or selected via cross-validation. For all columns, **smaller values are better**. Runtime reports the final comparison-stage fit (after estimating  $\widehat{\Sigma}$ ) and excludes initial tuning.

discussion on sensitivity). The proposed method is also computationally favorable.

We also conduct ablation studies, which reveal that each of Steps 1 and 2 in the proposed method play a crucial role. We report ROC curves regarding precision matrix estimation in [Figure 3](#). In particular, without clustering in Step 1, the observed dependence due to the latent class confounding invalidates the block structure estimation in Step 2 (leading to a non-informative ARI of 0.01), and results in a very low TPR. When the block structure estimation in Step 2 is omitted, the off-block entries of the precision matrix are subject to spurious false discovery, as indicated by the lower ROC curves.

## 5 Real Data Applications

### 5.1 ANES public opinion survey

We analyze the 2022 American National Election Studies (ANES) public opinion pilot survey ([American National Election Studies, 2022](#)). After preprocessing as in [Chen et al. \(2026\)](#), the dataset contains ordinal responses from  $N = 1511$  participants to  $J = 144$  items. The response categories  $C_j$  varies from 2 to 7; see [Figure 12](#) in the Supplement for a histogram.

Public opinion surveys often violate local independence because the questionnaire design creates dependent item groups. For example, the ANES survey has four consecutive questions

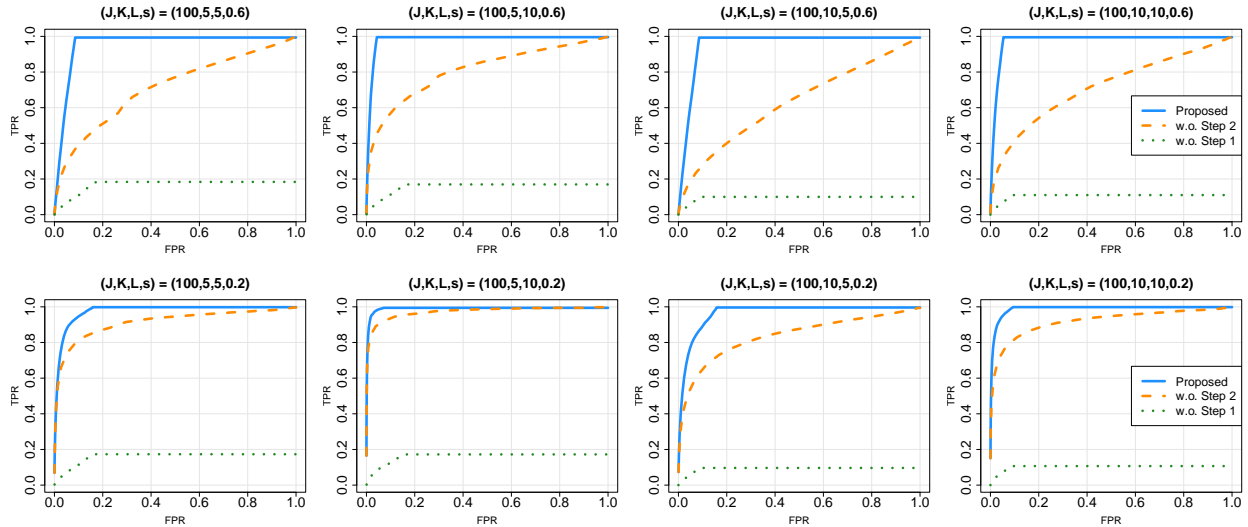


Figure 3: ROC curves (false positive rate versus true positive rate) for selecting  $\Omega$  under  $J = 100$  and varying other dimensions/sparsity. The solid line corresponds to the proposed method, whereas the dashed/dotted line corresponds to variants where Steps 2/1 are omitted, respectively.

that ask respondents whether being White, Black, Hispanic, or Asian comes with advantages (these correspond to nodes 5–8 in Figure 6). We show that our method can learn such blocks in a fully data-driven manner. The full data analysis using the proposed pipeline took 16 seconds, with 0.1, 1.8, and 13.7 seconds for Steps 1–3, respectively, including tuning parameter selection in Step 3. We discuss the findings step by step.

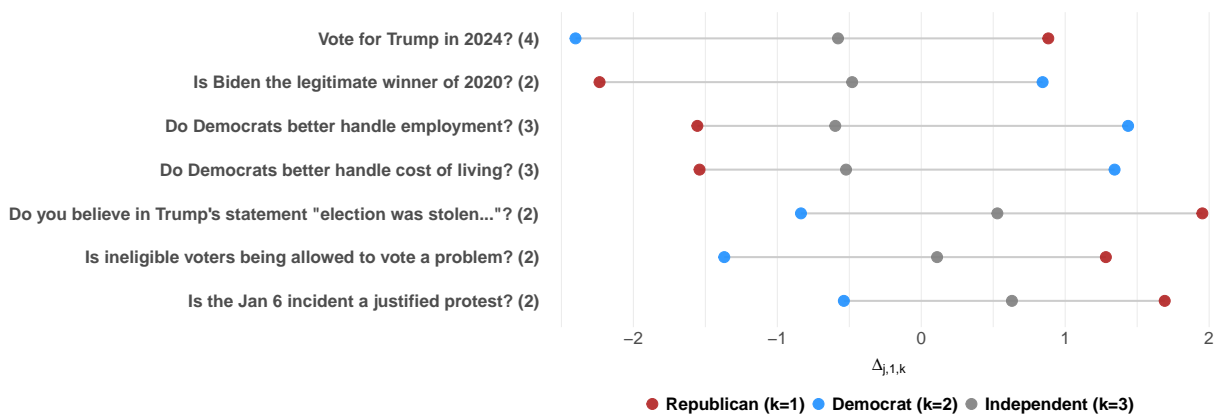


Figure 4: Visualization of the threshold parameter  $\Delta_{j,1,k}$  for sample ANES items. Each row corresponds to a sample item (number of categories  $C_j$  in parentheses), and each dot corresponds to each latent class  $k = 1, 2, 3$ . Note that  $\mathbb{P}(R_j = 1 \mid Z = k) = \Phi(\Delta_{j,1,k})$ .

**Step 1: clustering** We implemented Step 1 with  $K = 3$ ; see the Supplement for details. By inspecting the estimated threshold parameters  $\Delta_{j,1,k}$  for each cluster, the three clusters can be interpreted as Republican ( $k = 1$ ), Democrat ( $k = 2$ ), and Independent ( $k = 3$ ) voters. Example items are visualized in Figure 4, where the Republican and Democrat clusters typically form the two extremes. This interpretation validates the existence of latent classes and shows that spectral clustering can detect them.

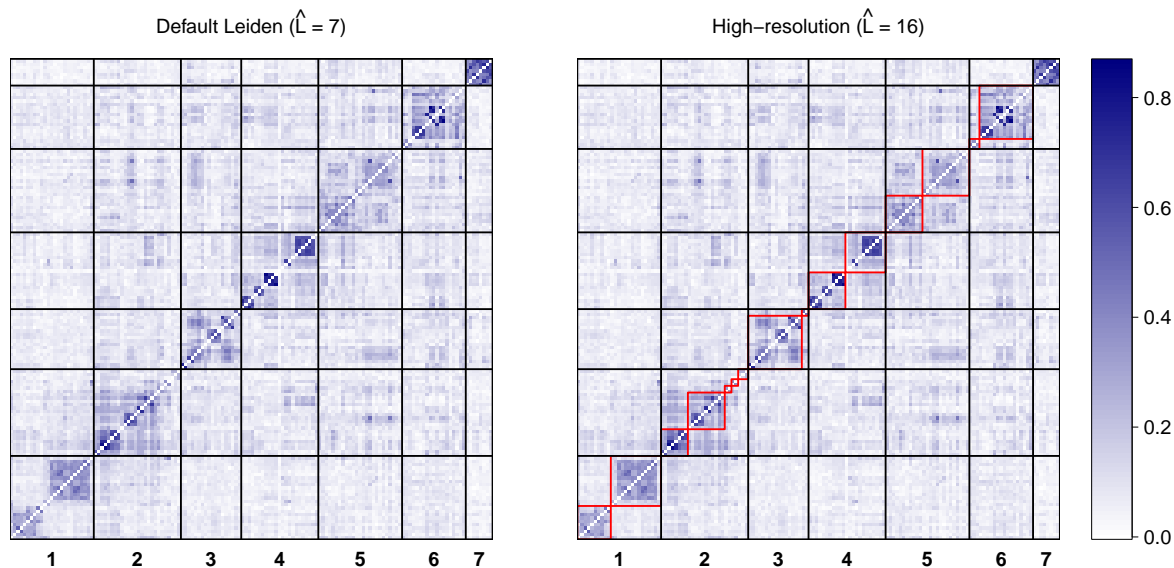


Figure 5: Learned ANES block structures at two resolutions. Both panels show the same thresholded matrix  $\tilde{\mathbf{G}}$  with identical row/column permutations; the left uses default Leiden, and the right uses resolution 1.5. Red lines indicate the additional fine-grained high-resolution blocks.

**Step 2: learning block structures** We applied our Step 2 with the continuous aggregation matrix  $\tilde{\mathbf{G}}$ . Figure 5 displays the learned block structures at two different algorithmic resolutions. In the left panel, we implemented the default Leiden algorithm, and the items are partitioned into  $\hat{L} = 7$  blocks. In the right panel, we increased the Leiden resolution parameter to 1.5, which gives  $\hat{L} = 16$  blocks. We see that most of the 7 blocks (in black) are partitioned into fine-grained sub-blocks (in red). Referring to the questionnaire allowed us to interpret each coarser and finer block (see the first/second columns of Table 3), revealing an interesting hierarchical structure. For instance, a coarse block on ‘issue importance’ is split into economic and social issues (see the fifth row in Table 3). This multi-resolution capability

Default Leiden	High-resolution	Example item (paraphrased)
1. Political Engagement	Participation	Joined in a protest march in the past year?
	Issue ownership	Do Democrats better handle “employment”?
2. Trust	President	Approve of Biden’s job as president?
	Experts	Do election officials try to advantage particular candidates?
	Jan 6 incident	Is the Jan 6 incident a justified protest?
	Elections	Do officials try to get election results right?
3. Racism	Political tolerance	Do you favor firing “gun rights activists”?
	Privileges/resentment	Does being “Asian” come with advantages?
4. Democratic Attitudes	Reasons	Differences due to “biological reasons”?
	Immigration	Do immigrants make you “angry”?
5. Issue Importance	Electoral integrity	Is Biden the legitimate winner of 2020?
	Economic	How important is the “taxes” issue?
6. Abortion	Social	How important is the “gun” issue?
	Prosecution	Do you favor prosecuting health care professionals who perform abortions?
	Emotions	Does Roe v. Wade being overturned make you feel “angry”?
7. Racial Stereotypes	—	Are “White” people hard-working?

Table 3: Hierarchical block structure of the ANES dataset across two algorithmic resolutions. The coarse blocks (left) partition into nuanced sub-blocks (middle) under a larger resolution parameter. Example word choices among multiple similar items are indicated in quote marks. The block index 1 – 7 in the first column matches that in Figure 5.

can be practically useful as it allows researchers to adjust the granularity of blocks easily.

For evaluation, we compute the ARI between  $\hat{V}$  and the questionnaire item groups. The questionnaire has  $L = 31$  groups, including 19 short blocks (with length four or less); see Table 6 in the Supplement. The default/high-resolution partitions in Figure 5 achieve ARI of 0.31 and 0.42. We note that the questionnaire groups are only a guideline rather than ground truth. Indeed, the seemingly mismatched entries are still highly interpretable. For example, the items “how worried are you about black citizens being the victims of violent crime” and “do you think public schools focus too much on race and racism?” are listed under the respective questionnaire categories of “crime” and “role of schools”. Both items are assigned to the “racism” block by our method, revealing nuanced dependence not captured by the default grouping.

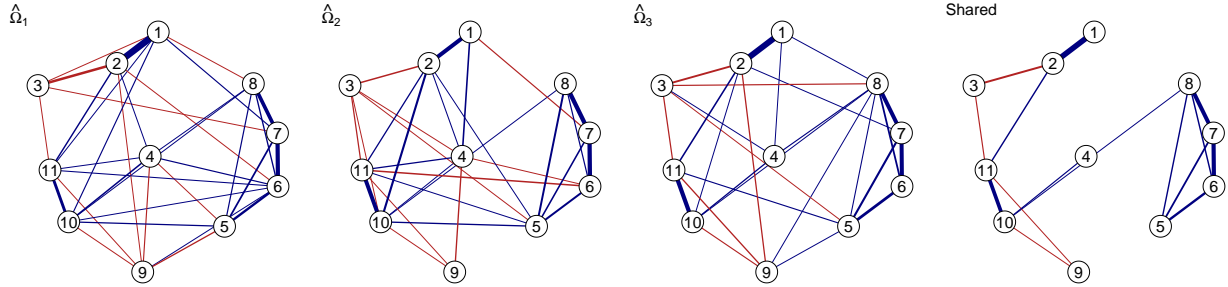


Figure 6: Estimated partial-correlation networks for selected nodes in ANES “racism” block. The first three panels correspond to the ‘Republican’, ‘Democrat’, and ‘Independent’ latent classes, and the last panel displays the shared edges. Edge width is proportional to partial correlation, with the blue/red colors denoting positive/negative values. Details of the 11 nodes are given in Table 7 in the Supplement.

**Step 3: precision matrix estimation** Fixing the block structure with  $\hat{L} = 7$ , we estimate the precision matrices  $\mathbf{\Omega}$ . Partial-correlation networks ( $\rho_{(j,j'),k} := -\omega_{(j,j'),k} / \sqrt{\omega_{(j,j),k}\omega_{(j',j'),k}}$ ) for selected nodes in the racism block  $V_3$  are displayed in Figure 6. For simpler presentation, the nodes are labeled as 1–11; see Table 7 in the Supplement for the node information.

The estimated networks show both shared and class-specific dependence. Among the 27, 25, and 22 edges in the first three graphs, 15 are shared. This includes the clique on nodes 5–8 about racial-group advantages for White/Black/Hispanic/Asian people. In contrast, we also see heterogeneous edges across the three classes. A notable discrepancy occurs at the edge 6–11, where the two nodes correspond to the items “do you think that being Black comes with advantages” and “over the past few years, Blacks have gotten less than they deserve”. In the more polarized latent classes (Republicans and Democrats; see the first two panels), these items exhibit conditional dependencies with different signs. However, the third latent class (Independents) exhibits conditional independence. A similar pattern appears for edge 1–7, illustrating how our method captures dependence differences across ideological clusters.

## 5.2 HapMap3 genetics data

We next analyze the HapMap3 dataset, which collects genotypes of individuals from different populations (Consortium et al., 2010). As the full dataset is extremely high-dimensional, we

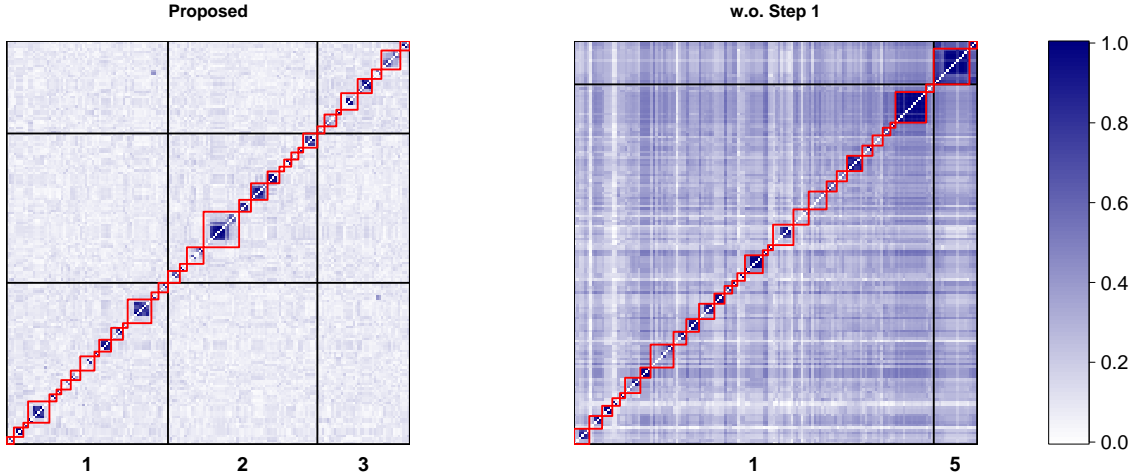


Figure 7: Estimated  $\tilde{\mathbf{G}}$  and community structures for the HapMap3 data. Black/red lines show the default/high-resolution blocks, respectively. Left: the proposed method (Steps 1 and 2). Right: a modified analysis that omits Step 1. The columns of each panel are permuted separately. The proposed analysis leaves much weaker dependence between different learned blocks, visible as lighter off-block regions.

focus on the  $J = 500$  single nucleotide polymorphisms (SNPs) on chromosome 22 with the largest variances. The observed genotype  $R_{i,j}$  is encoded as 0, 1, or 2, representing the count of a specific reference allele, so each SNP takes  $C_j = 3$  values. We study  $N = 479$  individuals from  $K = 4$  distinct subpopulations. See Supplement F.3 for additional discussion on why block structures are natural here.

Our method took 25 seconds to run, of which Step 1 took 0.1 seconds and Step 2 took 24.6 seconds. Because individual SNP-level dependencies are difficult to interpret biologically, we focus on block-structure recovery and do not report Step 3 for this dataset.

**Step 1: clustering** We applied Step 1 with  $K = 4$ . Compared to the held-out subpopulation information, clustering was nearly perfect, with 11 errors among the  $N = 479$  individuals. This illustrates the good performance of the proposed clustering procedure despite local dependence.

**Step 2: learning block structures** Next, we applied Step 2 to learn block structures. The left panel of Figure 7 shows the first three large default-resolution blocks, covering 157

SNPs. The default resolution selected  $\hat{L} = 11$  blocks, while the high-resolution run selected  $\hat{L} = 76$  finer blocks. The average absolute estimated covariance over off-block SNP pairs is similar under the default and high-resolution partitions: 0.086 and 0.087, respectively. Thus, the additional splits do not increase between-block dependence, supporting the use of the high-resolution partition. The estimated blocks mostly align with the sequential SNP ordering, although some non-adjacent SNPs are assigned to the same block.

Finally, we emphasize that accounting for the population heterogeneity in Step 1 is crucial. When the clustering in Step 1 is omitted, the right panel of Figure 7 shows much larger cross-block correlations. Quantitatively, the average off-block correlation is 0.287 without Step 1, compared with the value of 0.087 after conditioning on the estimated subpopulations.

## 6 Discussion

We have proposed an interpretable and theoretically grounded methodology that relaxes local independence in modern high-dimensional latent class analysis. We propose a block-dependent LCM and developed a practical and scalable algorithm that sequentially estimates all model components. The proposed method is supported by rigorous finite-sample theoretical guarantees as well as promising illustrations in both social and biological applications.

There are several interesting directions for further work. First, our theoretical consistency result builds upon exact recovery of latent classes and block structures. A natural extension is to investigate downstream estimation robustness under weak clustering recovery or block recovery. Methodologically, one may enhance Step 2 of our method by integrating robust polychoric correlation estimators (Welz et al., 2026), at additional computational cost.

Second, our current framework assumes fully observed responses, whereas many block-dependent ordinal datasets suffer from missingness. For instance, movie ratings may be dependent through shared genres or actors, but each user rates only a small fraction of movies. Hence, extending our methodology to accommodate missingness would be important.

Finally, our unsupervised framework can be naturally extended to supervised settings,

such as latent class regression with block-structured dependence, by incorporating covariates to the latent Gaussian mean in (3). Also, we can integrate mixed data types (such as continuous) by modifying the polychoric correlation estimator in Step 2 accordingly.

**Acknowledgements** This research is partially supported by NSF Grant DMS-2210796.

## References

- Abbe, E., Fan, J., and Wang, K. (2022). An  $\ell^p$  theory of PCA and spectral clustering. *The Annals of Statistics*, 50(4):2359–2385.
- American National Election Studies (2022). ANES 2022 Pilot Study [dataset and documentation]. December 14, 2022 version.
- Asparouhov, T. and Muthén, B. (2011). Using bayesian priors for more flexible latent class analysis. In *proceedings of the 2011 joint statistical meeting, Miami Beach, FL*. American Statistical Association Alexandria, VA.
- Asparouhov, T. and Muthén, B. (2015). Residual associations in latent class and latent transition analysis. *Structural Equation Modeling: A Multidisciplinary Journal*, 22(2):169–177.
- Barber, R. and Drton, M. (2010). Extended Bayesian information criteria for Gaussian graphical models. *Advances in neural information processing systems*, 23.
- Barrett, J. C., Fry, B., Maller, J., and Daly, M. J. (2005). Haploview: analysis and visualization of ld and haplotype maps. *Bioinformatics*, 21(2):263–265.
- Bassett, D. S., Wymbs, N. F., Porter, M. A., Mucha, P. J., Carlson, J. M., and Grafton, S. T. (2011). Dynamic reconfiguration of human brain networks during learning. *Proceedings of the National Academy of Sciences*, 108(18):7641–7646.
- Berisa, T. and Pickrell, J. K. (2015). Approximately independent linkage disequilibrium blocks in human populations. *Bioinformatics*, 32(2):283.
- Blondel, V. D., Guillaume, J.-L., Lambiotte, R., and Lefebvre, E. (2008). Fast unfolding of communities in large networks. *Journal of Statistical Mechanics: Theory and Experiment*, 2008(10):P10008.
- Bonett, D. G. and Price, R. M. (2005). Inferential methods for the tetrachoric correlation coefficient. *Journal of Educational and Behavioral Statistics*, 30(2):213–225.
- Braeken, J. (2011). A boundary mixture approach to violations of conditional independence. *Psychometrika*, 76(1):57–76.
- Braeken, J., Tuerlinckx, F., and De Boeck, P. (2007). Copula functions for residual dependency. *Psychometrika*, 72(3):393–411.
- Cai, T., Liu, W., and Luo, X. (2011). A constrained  $\ell_1$  minimization approach to sparse precision matrix estimation. *Journal of the American Statistical Association*, 106(494):594–607.

- Chandrasekaran, V., Parrilo, P. A., and Willsky, A. S. (2012). Latent variable graphical model selection via convex optimization. *The Annals of Statistics*, 40(4):1935 – 1967.
- Chatterjee, A., Nandy, S., and Sadhu, R. (2024). Detecting planted partition in sparse multilayer networks. *Information and Inference: A Journal of the IMA*, 13(3):iaae019.
- Chen, J. and Chen, Z. (2008). Extended Bayesian information criteria for model selection with large model spaces. *Biometrika*, 95(3):759–771.
- Chen, L., Huang, C., and Gu, Y. (2026). Generalized grade-of-membership estimation for high-dimensional locally dependent data. *Journal of the American Statistical Association*, (just-accepted):1–28.
- Chen, Y., Chi, Y., Fan, J., and Ma, C. (2021). Spectral methods for data science: A statistical perspective. *Foundations and Trends in Machine Learning*, 14(5):566–806.
- Chen, Y., Li, X., Liu, J., and Ying, Z. (2018). Robust measurement via a fused latent and graphical item response theory model. *Psychometrika*, 83(3):538–562.
- Consortium, I. H. . et al. (2010). Integrating common and rare genetic variation in diverse human populations. *Nature*, 467(7311):52.
- Danaher, P., Wang, P., and Witten, D. M. (2014). The joint graphical lasso for inverse covariance estimation across multiple classes. *Journal of the Royal Statistical Society Series B: Statistical Methodology*, 76(2):373–397.
- Dendukuri, N. and Joseph, L. (2001). Bayesian approaches to modeling the conditional dependence between multiple diagnostic tests. *Biometrics*, 57(1):158–167.
- Everitt, B. S. (1988). A finite mixture model for the clustering of mixed-mode data. *Statistics & Probability Letters*, 6(5):305–309.
- Fan, J., Liu, H., Ning, Y., and Zou, H. (2017). High dimensional semiparametric latent graphical model for mixed data. *Journal of the Royal Statistical Society Series B: Statistical Methodology*, 79(2):405–421.
- Feng, H. and Ning, Y. (2019). High-dimensional mixed graphical model with ordinal data: Parameter estimation and statistical inference. In *The 22nd International Conference on Artificial Intelligence and Statistics*, pages 654–663. PMLR.
- Fortunato, S. and Barthelemy, M. (2007). Resolution limit in community detection. *Proceedings of the National Academy of Sciences*, 104(1):36–41.
- Friedman, J., Hastie, T., and Tibshirani, R. (2008). Sparse inverse covariance estimation with the graphical lasso. *Biostatistics*, 9(3):432–441.
- Frot, B., Jostins, L., and McVean, G. (2019a). Graphical model selection for Gaussian conditional random fields in the presence of latent variables. *Journal of the American Statistical Association*.
- Frot, B., Nandy, P., and Maathuis, M. H. (2019b). Robust causal structure learning with some hidden variables. *Journal of the Royal Statistical Society Series B: Statistical Methodology*, 81(3):459–487.
- Gabriel, S. B., Schaffner, S. F., Nguyen, H., Moore, J. M., Roy, J., Blumenstiel, B., Higgins, J., DeFelice, M., Lochner, A., Faggart, M., et al. (2002). The structure of haplotype blocks in the human genome. *Science*, 296(5576):2225–2229.

- Gordon, S. L., Mazaheri, B., Rabani, Y., and Schulman, L. (2023). Causal inference despite limited global confounding via mixture models. In *Conference on Causal Learning and Reasoning*, pages 574–601. PMLR.
- Greene, D. and Cunningham, P. (2013). Producing a unified graph representation from multiple social network views. In *Proceedings of the 5th annual ACM web science conference*, pages 118–121.
- Guo, J., Levina, E., Michailidis, G., and Zhu, J. (2011). Joint estimation of multiple graphical models. *Biometrika*, 98(1):1–15.
- Guo, J., Levina, E., Michailidis, G., and Zhu, J. (2015). Graphical models for ordinal data. *Journal of Computational and Graphical Statistics*, 24(1):183–204.
- Hagenaars, J. A. (1988). Latent structure models with direct effects between indicators: local dependence models. *Sociological Methods & Research*, 16(3):379–405.
- Harper, D. (1972). Local dependence latent structure models. *Psychometrika*, 37(1):53–59.
- Hermes, S., van Heerwaarden, J., and Behrouzi, P. (2024). Copula graphical models for heterogeneous mixed data. *Journal of Computational and Graphical Statistics*, 33(3):991–1005.
- Hubert, L. and Arabie, P. (1985). Comparing partitions. *Journal of Classification*, 2(1):193–218.
- Ketchen, D. J. and Shook, C. L. (1996). The application of cluster analysis in strategic management research: an analysis and critique. *Strategic management journal*, 17(6):441–458.
- Kim, S. A., Cho, C.-S., Kim, S.-R., Bull, S. B., and Yoo, Y. J. (2018). A new haplotype block detection method for dense genome sequencing data based on interval graph modeling of clusters of highly correlated snps. *Bioinformatics*, 34(3):388–397.
- Korpershoek, H., Kuyper, H., and van der Werf, G. (2015). Differences in students’ school motivation: A latent class modelling approach. *Social Psychology of Education*, 18(1):137–163.
- Lancaster, H. and Hamdan, M. (1964). Estimation of the correlation coefficient in contingency tables with possibly nonmetrical characters. *Psychometrika*, 29(4):383–391.
- Lazarsfeld, P. F. (1950). The logical and mathematical foundation of latent structure analysis. *Studies in social psychology in world war II Vol. IV: Measurement and prediction*, pages 362–412.
- Lee, J., Jung, K., and Park, J. (2020). Detecting conditional dependence using flexible bayesian latent class analysis. *Frontiers in Psychology*, 11:1987.
- Lee, K. H., Chen, Q., DeSarbo, W. S., and Xue, L. (2022). Estimating finite mixtures of ordinal graphical models. *Psychometrika*, 87(1):83–106.
- Lee, S. and Gu, Y. (2026). Deep discrete encoders: Identifiable deep generative models for rich data with discrete latent layers. *Journal of the American Statistical Association*, 121(553):194–208.
- Lee, S., Mukherjee, R., and Mukherjee, S. (2025). Inference on Gaussian mixture models with dependent labels. *arXiv preprint arXiv:2510.06501*.
- Lee, W. and Liu, Y. (2015). Joint estimation of multiple precision matrices with common structures. *The Journal of Machine Learning Research*, 16(1):1035–1062.
- Liu, H., Han, F., Yuan, M., Lafferty, J., and Wasserman, L. (2012). High-dimensional semipara-

- metric Gaussian copula graphical models. *The Annals of Statistics*, pages 2293–2326.
- Liu, H., Lafferty, J., and Wasserman, L. (2009). The nonparanormal: Semiparametric estimation of high dimensional undirected graphs. *Journal of Machine Learning Research*, 10(10).
- Liu, Y., Darville, T., Zheng, X., and Li, Q. (2023). Decomposition of variation of mixed variables by a latent mixed Gaussian copula model. *Biometrics*, 79(2):1187–1200.
- Lyu, Z., Chen, L., and Gu, Y. (2025). Degree-heterogeneous latent class analysis for high-dimensional discrete data. *Journal of the American Statistical Association*, 120(552):2435–2448.
- Lyu, Z. and Gu, Y. (2026). Spectral clustering with likelihood refinement for high-dimensional latent class recovery. *Psychometrika*, page 1–45.
- Ma, J. and Michailidis, G. (2016). Joint structural estimation of multiple graphical models. *Journal of Machine Learning Research*, 17(166):1–48.
- Ma, Z. and Nandy, S. (2023). Community detection with contextual multilayer networks. *IEEE Transactions on Information Theory*, 69(5):3203–3239.
- Magidson, J., Vermunt, J. K., and Madura, J. P. (2020). *Latent class analysis*, volume 714. SAGE Publications Limited Thousand Oaks, CA, USA:.
- Marsman, M., van den Bergh, D., and Haslbeck, J. M. (2025). Bayesian analysis of the ordinal markov random field. *Psychometrika*, 90(1):146–182.
- Mazaheri, B., Gordon, S., Rabani, Y., and Schulman, L. (2023). Causal discovery under latent class confounding. *arXiv preprint arXiv:2311.07454*.
- Menten, J., Boelaert, M., and Lesaffre, E. (2008). Bayesian latent class models with conditionally dependent diagnostic tests: a case study. *Statistics in medicine*, 27(22):4469–4488.
- Miao, Z., Chen, Y.-C., and Dobra, A. (2024). Bayesian finite mixtures of ising models. *Metrika*, pages 1–33.
- Mohan, K., London, P., Fazel, M., Witten, D., and Lee, S.-I. (2014). Node-based learning of multiple Gaussian graphical models. *The Journal of Machine Learning Research*, 15(1):445–488.
- Muthén, B. (1984). A general structural equation model with dichotomous, ordered categorical, and continuous latent variable indicators. *Psychometrika*, 49(1):115–132.
- Olsson, U. (1979). Maximum likelihood estimation of the polychoric correlation coefficient. *Psychometrika*, 44(4):443–460.
- Paul, S. and Chen, Y. (2020). Spectral and matrix factorization methods for consistent community detection in multi-layer networks. *The Annals of Statistics*, 48(1):230–250.
- Pearson, K. (1900). I. mathematical contributions to the theory of evolution.—vii. on the correlation of characters not quantitatively measurable. *Philosophical Transactions of the Royal Society of London. Series A*, 195(262-273):1–47.
- Qu, Y., Tan, M., and Kutner, M. H. (1996). Random effects models in latent class analysis for evaluating accuracy of diagnostic tests. *Biometrics*, pages 797–810.
- Quan, X., Booth, J. G., and Wells, M. T. (2018). Rank-based approach for estimating correlations in mixed ordinal data. *arXiv preprint arXiv:1809.06255*.

- Rothman, A. J., Bickel, P. J., Levina, E., and Zhu, J. (2008). Sparse permutation invariant covariance estimation. *Electronic Journal of Statistics*, 2(none):494 – 515.
- Rousseeuw, P. J. (1987). Silhouettes: a graphical aid to the interpretation and validation of cluster analysis. *Journal of computational and applied mathematics*, 20:53–65.
- Thorndike, R. L. (1953). Who belongs in the family? *Psychometrika*, 18(4):267–276.
- Traag, V. A., Aldecoa, R., and Delvenne, J.-C. (2015). Detecting communities using asymptotical surprise. *Physical review e*, 92(2):022816.
- Traag, V. A., Waltman, L., and Van Eck, N. J. (2019). From Louvain to Leiden: guaranteeing well-connected communities. *Scientific reports*, 9(1):5233.
- Uebersax, J. S. (1999). Probit latent class analysis with dichotomous or ordered category measures: Conditional independence/dependence models. *Applied Psychological Measurement*, 23(4):283–297.
- Vacek, P. M. (1985). The effect of conditional dependence on the evaluation of diagnostic tests. *Biometrics*, pages 959–968.
- Van der Vaart, A. W. (2000). *Asymptotic statistics*, volume 3. Cambridge university press.
- Vermunt, J. K. and Magidson, J. (2002). Latent class cluster analysis. *Applied latent class analysis*, 11(89-106):60.
- Vershynin, R. (2018). *High-dimensional probability: An introduction with applications in data science*, volume 47. Cambridge university press.
- Wang, M. and Hanges, P. J. (2011). Latent class procedures: Applications to organizational research. *Organizational Research Methods*, 14(1):24–31.
- Welz, M., Mair, P., and Alfons, A. (2026). Robust estimation of polychoric correlation. *Psychometrika*, 91(1):247–278.
- Xie, F., Huang, B., Chen, Z., Cai, R., Glymour, C., Geng, Z., and Zhang, K. (2024). Generalized independent noise condition for estimating causal structure with latent variables. *Journal of Machine Learning Research*, 25(191):1–61.
- Yang, S., Lu, Z., Shen, X., Wonka, P., and Ye, J. (2015). Fused multiple graphical lasso. *SIAM Journal on Optimization*, 25(2):916–943.
- Yoo, Y. J., Kim, S. A., and Bull, S. B. (2015). Clique-based clustering of correlated snps in a gene can improve performance of gene-based multi-bin linear combination test. *BioMed Research International*, 2015(1):852341.
- Yoon, G., Carroll, R. J., and Gaynanova, I. (2020). Sparse semiparametric canonical correlation analysis for data of mixed types. *Biometrika*, 107(3):609–625.
- Yuan, M. and Lin, Y. (2007). Model selection and estimation in the Gaussian graphical model. *Biometrika*, 94(1):19–35.
- Yueh, W.-C. (2005). Eigenvalues of several tridiagonal matrices. *Applied Mathematics E-Notes [electronic only]*, 5:66–74.
- Zhang, A. Y. and Zhou, H. Y. (2024). Leave-one-out singular subspace perturbation analysis for spectral clustering. *The Annals of Statistics*, 52(5):2004–2033.

# Supplement to “Beyond Local Independence: High-Dimensional Latent Class Graphical Models with Shared Block Structure”

The supplement is organized as follows. Section [A](#) discusses related work on locally dependent latent class models, Gaussian graphical and copula models, and other models. Section [B](#) proves all main results from Section [3](#), and Section [C](#) proves auxiliary lemmas. Section [D](#) describes implementation details regarding simulations. Section [E](#) presents additional comparison studies and visualizations, including a likelihood-based refinement procedure for clustering. Section [F](#) provides additional details and discussion regarding the real data analysis.

## A Additional Related Work

**Locally dependent latent class models** There is a steady line of methodological work from quantitative social science and medical diagnosis on relaxing the local independence assumption in LCMS. One classical approach is to directly add pairwise or higher-order interaction effects while modeling the conditional probabilities, assuming a known dependence graph or considering all second-order interactions ([Harper, 1972](#); [Hagenaars, 1988](#); [Asparouhov and Muthén, 2015](#)). Another classical approach is to introduce a unidimensional latent Gaussian random-effect to model dependence in each class ([Qu et al., 1996](#); [Dendukuri and Joseph, 2001](#); [Menten et al., 2008](#)). This line of random-effect modeling has been especially popular in medicine to model conditionally dependent test results.

More related to our work, [Everitt \(1988\)](#) and [Uebersax \(1999\)](#) formulated the probit latent class framework (see [\(3\)–\(4\)](#)) for binary and ordinal data. This model has served as a baseline model for developing both Bayesian and frequentist methods that accommodate local dependence ([Asparouhov and Muthén, 2011](#); [Lee et al., 2020, 2022](#)). See [Lee et al. \(2022\)](#) for additional references. In the most general framework, [Uebersax \(1999\)](#) allowed

the threshold vector  $\Delta$  to vary across classes as in (4), but later works often considered homogeneous thresholds shared across latent classes. A more important distinction is that all cited works are methodologically driven under a fixed  $J$ . The Bayesian methods mainly focus on MCMC sampling and the frequentist methods are based on EM algorithms to compute the marginal maximum likelihood estimator, both of which can be concerning when  $J$  is large. Our work fills in this gap by proposing a more computationally appealing method with solid theoretical guarantees regarding learning the dependence structure for high-dimensional data with increasing  $J$ .

**Gaussian graphical models, copulas, and network models** Gaussian graphical models and copulas (also called nonparanormals) have been studied extensively to model dependent continuous data (Yuan and Lin, 2007; Liu et al., 2009, 2012). To allow various response types, extensions have been proposed for binary data (Fan et al., 2017) as well as ordinal/mixed data (Guo et al., 2015; Feng and Ning, 2019; Quan et al., 2018) and truncated data (Yoon et al., 2020). However, the vast majority of these works do not consider *heterogeneous latent sources*, as considered in this paper. Note that ignoring potential latent classes and fitting a single graphical model may lead to inconsistent estimation, and it is important to model such heterogeneous populations. Also, most methods (excluding Guo et al. (2015), which proposes a variational EM algorithm) rely on Kendall’s tau as discussed in Remark 1. A few exceptions include Chandrasekaran et al. (2012); Frot et al. (2019b,a), which take a different approach from ours by using linear structural equations to model the relationship between continuous latent variables and observations.

We also note another line of work that assumes knowledge of the heterogeneous sources (that is, with fully observed class labels) and posits separate Gaussian graphical models for each source (Guo et al., 2011; Danaher et al., 2014; Lee and Liu, 2015; Ma and Michailidis, 2016). In particular, Guo et al. (2011) considers a related notion of shared sparsity across sources, but without block structures. Ma and Michailidis (2016) assumed prior knowledge of the structural relationship between multiple graphical models. Danaher et al. (2014),

Mohan et al. (2014), and Yang et al. (2015) used a shared block structure among the multiple precision matrix estimates to speed up computation. Unlike this paper, the block structure in the above studies is not an interpretable modeling assumption to capture unobserved population heterogeneity, but is a structural artifact that arises from solving a strongly penalized optimization problem, so the estimated structure crucially depends on the penalty parameter. Extending such Gaussian likelihood-based methods to ordinal data is non-trivial, and we instead estimate the block structure directly from the covariance matrices (instead of simultaneously learning the precision matrices). This way, we can circumvent introducing an additional joint penalty regarding the similarity of precision matrices. More recent works also considered multiple graphical models using Gaussian copulas (Liu et al., 2023; Hermes et al., 2024).

Additionally, continuous latent variable models based on non-Gaussian copulas have been proposed in the item response theory literature in psychometrics (Braeken et al., 2007; Braeken, 2011). These works also consider similar block structures within the items, but assume that the block structure is known. Focusing exclusively on binary data, latent variable network models based on non-Gaussian graphical modeling (such as Ising models) have also been introduced (Chen et al., 2018; Miao et al., 2024), and have been recently extended to ordinal data as well (Marsman et al., 2025). However, these works assume the network dependence to be invariant with respect to the latent variables, and the estimation methods do not come with theoretical guarantees.

**Directed graphical models** This paper generalizes the usual latent class model by allowing *undirected* dependence structures among the observations, and we compare it with work in mixture modeling and causal discovery that considers *directed* dependence. While this problem has been popular for continuous data with linear structural equations (Chandrasekaran et al., 2012; Xie et al., 2024), discrete data has received less attention. Recently, Gordon et al. (2023), Mazaheri et al. (2023), and Lee and Gu (2026) considered a directed analog of the problem studied here, where the first two focus mainly on binary responses, and

the third allows more complex latent structures but under a generalized linear parametrization. This line of work treats the causal graph among the observed variables as fixed across latent classes, whereas our framework allows the within-block graph to vary. Also, their theoretical framework focuses on asymptotic population identifiability, whereas we establish non-asymptotic error bounds and allow high-dimensional responses.

**Multi-layer networks** Our model can also be viewed through the lens of multi-layer networks: each latent class induces a weighted graphical model with precision matrix  $\mathbf{\Omega}_k$  on the same items  $V = [J]$ . The within-block edges may vary across latent classes, but the target block partition is shared across layers. This connects our block-recovery step to work on planted partitions in multi-layer networks, which has been of both theoretical interest (in the context of multiple stochastic block models) (Paul and Chen, 2020; Ma and Nandy, 2023; Chatterjee et al., 2024) and applied interest (for brain and social networks) (Bassett et al., 2011; Greene and Cunningham, 2013). One distinction is that those works typically observe binary adjacency matrices, whereas here the weighted layer-specific graphs are estimated from tabular ordinal responses.

## B Proof of Main Results

### B.1 Proof of results from Section 3.1

*Proof of Proposition 1.* For simplicity, set  $\tilde{J} := \sum_{j=1}^J C_j$ . We equivalently write (8) as

$$\tilde{R}_{i, \sum_{m=0}^{j-1} C_{m+a}} = \theta_{j,a,k} + \epsilon_{i, \sum_{m=0}^{j-1} C_{m+a}},$$

where  $\epsilon_i = (\epsilon_{i,1}, \dots, \epsilon_{i,\tilde{J}})^\top \in [-1, 1]^{\tilde{J}}$  is a mean-zero noise vector that is independent across  $i$ . Under the block structure assumption, we can decompose  $\epsilon_i$  into  $L$  independent components  $(\epsilon_i^{(1)}, \dots, \epsilon_i^{(L)})$ . Then, denoting  $\|\cdot\|_{\psi_2}$  as the sub-Gaussian norm of a random vector (see

Definition 2.5.6, [Vershynin \(2018\)](#)), we have

$$\|\boldsymbol{\epsilon}_i\|_{\psi_2} = \max_{\ell=1}^L \|\boldsymbol{\epsilon}_i^{(\ell)}\|_{\psi_2} \leq \sqrt{\tilde{J}_{\max}},$$

so the mean-zero noise  $\boldsymbol{\epsilon}_i$  is sub-Gaussian with norm bounded by  $\sqrt{\tilde{J}_{\max}}$ . Here, the last inequality follows as  $\boldsymbol{\epsilon}_i^{(\ell)}$  is a bounded random vector with dimension  $\sum_{j \in V_\ell} C_j \leq \tilde{J}_{\max}$ .

Given the sub-Gaussian bound for the noise, we show (11) by invoking [Zhang and Zhou \(2024\)](#). Set the minimum distance between the cluster centers as

$$D_\theta := \min_{k \neq k' \in [K]} \|\boldsymbol{\theta}_k - \boldsymbol{\theta}_{k'}\|,$$

where  $\boldsymbol{\theta}_k = (\theta_{1,1,k}, \dots, \theta_{J,C_J,k})^\top$  denotes the flattened mean vector of the  $k$ th cluster. We first show that the associated signal-to-noise ratios in [Zhang and Zhou \(2024\)](#) are large enough:

$$\psi_1 := \frac{D_\theta}{K(1 + \sqrt{J/N})\sqrt{\tilde{J}_{\max}}} > c, \quad \rho_1 := \frac{\sigma_K(\mathbb{E}[\tilde{\mathbf{R}} | \mathbf{Z}])}{(\sqrt{N} + \sqrt{J})\sqrt{\tilde{J}_{\max}}} > c. \quad (17)$$

Below, we separately show each claim of (17) under the assumption

$$D \gtrsim K\sqrt{\tilde{J}_{\max}}\left(1 + \sqrt{\frac{J}{N}}\right), \quad \sigma_K(\boldsymbol{\Theta}) \gtrsim \sqrt{K\tilde{J}_{\max}}\left(1 + \sqrt{\frac{J}{N}}\right).$$

For showing the second bound in (17), we work under a high probability set  $E_1 := \{\min_{k \in [K]} N_k > \frac{\delta_3 N}{2K}\}$ , where  $N_k := \sum_{i=1}^N \mathbb{I}(Z_i = k)$  denotes the size of the  $k$ th latent class and  $\delta_3$  is the constant from Assumption 3. By the multiplicative Chernoff bound for the sum of bounded random variables, we get

$$\mathbb{P}\left(N_k \leq \frac{N\pi_k}{2}\right) = \mathbb{P}\left(N_k \leq \frac{\mathbb{E}[N_k]}{2}\right) \leq \exp\left(-\frac{N\pi_k}{8}\right).$$

Using  $\pi_k \geq \delta_3/K$  from Assumption 3 and a union bound, we have

$$\mathbb{P}(E_1^c) \leq \sum_{k=1}^K \mathbb{P}\left(N_k \leq \frac{N\pi_k}{2}\right) \leq K \exp\left(-\frac{\delta_3 N}{8K}\right). \quad (18)$$

As  $\mathbf{Y}$  is the  $N \times K$  one-hot membership matrix, we have  $\mathbf{Y}^\top \mathbf{Y} = \text{diag}(N_1, \dots, N_K)$ . Hence,

on  $E_1$ ,

$$\sigma_K(\mathbf{Y}) = \sqrt{\min_{k \in [K]} N_k} \geq \sqrt{\delta_3 N / 2K}.$$

Recalling the decomposition  $\mathbb{E}[\tilde{\mathbf{R}} \mid \mathbf{Z}] = \mathbf{Y}\Theta^\top$ , we have

$$\sigma_K(\mathbb{E}[\tilde{\mathbf{R}} \mid \mathbf{Z}]) \geq \sigma_K(\mathbf{Y})\sigma_K(\Theta) \gtrsim (\sqrt{N} + \sqrt{J})\sqrt{\tilde{J}_{\max}}.$$

Here, the first inequality is a standard fact regarding singular values, and the second inequality follows from invoking the assumption on  $\sigma_K(\Theta)$ .

Next, to show the first bound in (17), it suffices to prove that  $D_\theta \gtrsim D = \min_{k \neq k' \in [K]} \|\Delta_k - \Delta_{k'}\|$ , since the separation in the proposition is defined in terms of the threshold vectors  $\Delta_k$  as opposed to the cluster-center vectors  $\theta_k$ . Fix any  $k \neq k' \in [K]$  and define

$$d_{j,a} = d_{j,a,k,k'} := \Phi(\Delta_{j,a,k}) - \Phi(\Delta_{j,a,k'}), \quad \forall a \in [C_j - 1],$$

and  $\mathbf{d}_j = (d_{j,1}, \dots, d_{j,C_j-1})^\top$ . For notational convenience, also let  $d_{j,0} = d_{j,C_j} = 0$  so that

$$\theta_{j,a,k} - \theta_{j,a,k'} = d_{j,a} - d_{j,a-1}.$$

Hence, we have

$$\|\theta_{j,k} - \theta_{j,k'}\|^2 = \sum_{a=1}^{C_j} (d_{j,a} - d_{j,a-1})^2 = \mathbf{d}_j^\top \mathbf{A} \mathbf{d}_j,$$

where  $\mathbf{A}$  is a  $(C_j - 1) \times (C_j - 1)$  tri-diagonal matrix with 2 on the main diagonal and  $-1$  on the off-diagonals. Noting that  $\lambda_{\min}(\mathbf{A}) = 2 - 2\cos(\pi/C_j) > 0$  (see [Yueh \(2005\)](#)), we can write

$$\|\theta_{j,k} - \theta_{j,k'}\|^2 \gtrsim \|\mathbf{d}_j\|^2 \gtrsim \|\Delta_{j,k} - \Delta_{j,k'}\|^2,$$

so the claim holds. Here, the hidden constant in the  $\gtrsim$  symbols depend on  $C_{\max}$  and  $M$ , respectively.

Finally, we complete the proof. By intersecting on  $E_1$  and using Theorem 3.1 from [Zhang and Zhou \(2024\)](#) (note that their loss function is with a  $1/N$  scaling, also the condition

$N \gtrsim K^2$  is required for this result), we have

$$\begin{aligned} \mathbb{E}[\ell(\widehat{\mathbf{Z}}, \mathbf{Z}) \mid \mathbf{Z}] &= \mathbb{E}[\ell(\widehat{\mathbf{Z}}, \mathbf{Z})\mathbb{I}(\mathbf{Z} \in E_1) \mid \mathbf{Z}] + \mathbb{E}[\ell(\widehat{\mathbf{Z}}, \mathbf{Z})\mathbb{I}(\mathbf{Z} \in E_1^c) \mid \mathbf{Z}] \\ &\leq N \left( e^{-(1-c_2/\psi_1-c_2/\rho_1^2)\frac{D_\theta^2}{8J_{\max}}} + e^{-\frac{N}{2}} \right) + N\mathbb{I}(\mathbf{Z} \in E_1^c) \\ &\leq N \left( e^{-c_3\frac{D^2}{J_{\max}}} + e^{-\frac{N}{2}} \right) + N\mathbb{I}(\mathbf{Z} \in E_1^c). \end{aligned}$$

Here, the last line used (17) and  $D_\theta \gtrsim D$ . Now, (11) follows from taking an outer expectation over  $\mathbf{Z}$ , and using the bound (18). Here, note that the middle term is dominated by (18).  $\square$

*Proof of Proposition 2.* We first show the bound for  $\boldsymbol{\pi}$ . By intersecting with the event of exact clustering  $E_2 := \{\widehat{\mathbf{Z}} = \mathbf{Z}\}$  (for simplicity, assume that the labels are correctly permuted), we have

$$\begin{aligned} \mathbb{P}(\max_{k \in [K]} |\widehat{\pi}_k - \pi_k| \geq t) &\leq \mathbb{P}\left(\max_{k \in [K]} \left| \frac{1}{N} \sum_{i=1}^N \mathbb{I}(Z_i = k) - \pi_k \right| \geq t\right) + p_1 \\ &\leq \sum_{k=1}^K \mathbb{P}\left(\left| \frac{1}{N} \sum_{i=1}^N \mathbb{I}(Z_i = k) - \pi_k \right| \geq t\right) + p_1 \leq 2Ke^{-2Nt^2} + p_1. \end{aligned}$$

For the first inequality, we used Proposition 1 to get  $\mathbb{P}(E_2^c) \leq p_1$  ( $p_1$  is as in (11)). The second inequality follows from a union bound, and the final inequality follows from Hoeffding's inequality (see Theorem 2.2.6 in Vershynin (2018)).

Next, we show the bound for  $\boldsymbol{\Delta}$ . We work under  $E_1$  and  $E_2$ , where  $E_1$  is as in the proof of Proposition 1. For any  $t < M$ , by intersecting with  $E_1, E_2$ , we have

$$\begin{aligned} \mathbb{P}(\sup_{j,a,k} |\widehat{\Delta}_{j,a,k} - \Delta_{j,a,k}| > t) &\leq \sum_{j,a,k} \mathbb{P}(|\widehat{\Delta}_{j,a,k} - \Delta_{j,a,k}| > t, E_1, E_2) + \mathbb{P}(E_1^c) + \mathbb{P}(E_2^c) \\ &\leq \sum_{j,a,k} \mathbb{P}\left(\left| \frac{1}{\widehat{N}_k} \sum_{i: \widehat{Z}_i=k} \mathbb{I}(R_{i,j} \leq a) - \Phi(\Delta_{j,a,k}) \right| > \frac{t}{M}, E_1, E_2\right) + Ke^{-cN/K} + p_1 \\ &\leq \sum_{j,a,k} \mathbb{P}\left(\left| \frac{1}{N_k} \sum_{i: Z_i=k} \mathbb{I}(R_{i,j} \leq a) - \Phi(\Delta_{j,a,k}) \right| > \frac{t}{M}, E_1\right) + p_1 \\ &\leq \sum_{j,a,k} 2\mathbb{E}\left[\exp\left(-\frac{2N_k t^2}{M^2}\right)\mathbb{I}(E_1)\right] + p_1 \\ &\leq 2\left(\sum_{j=1}^J C_j\right)Ke^{-\frac{2ct^2}{M^2}\frac{N}{K}} + p_1. \end{aligned}$$

Here, the first inequality follows from a union bound. The second line uses (i) the fact that the function  $\Phi^{-1}$  is  $M'$ -Lipschitz with  $M' = 1/\phi(2M)$  under the domain  $[\Phi(-2M), \Phi(2M)]$  (cf. Lemma A.1 in [Fan et al. \(2017\)](#)), (ii) the bounds for  $E_1, E_2$  from Proposition 1. The third line uses the definition of  $E_2$  alongside  $p_1 \gtrsim Ke^{-cN/K}$ , and the fourth line follows from the tower property and Hoeffding's inequality (conditioned on  $\mathbf{Z}$ ). The final line follows from using the definition of  $E_1$  to lower bound each  $N_k$ . This gives the desired bound.  $\square$

## B.2 Proof of results from Section 3.2

We prove Proposition 3 using the following lemma regarding finite-sample error bounds for pairwise polychoric correlations. In the statement of the lemma, we use a simplified notation by setting  $j = 1, j' = 2$  and omitting the latent class index  $k$ .

**Lemma 1.** Assume  $\begin{pmatrix} X_1^{(\rho)} \\ X_2^{(\rho)} \end{pmatrix} \sim N\left(\begin{pmatrix} 0 \\ 0 \end{pmatrix}, \begin{pmatrix} 1 & \rho \\ \rho & 1 \end{pmatrix}\right)$ , where  $|\rho| \leq 1 - \delta_1$ . For  $a \in [C_1], b \in [C_2]$ , let

$$\pi_{a,b}(\rho; \Delta_1, \Delta_2) := \mathbb{P}(X_1^{(\rho)} \in [\Delta_{1,a-1}, \Delta_{1,a}), X_2^{(\rho)} \in [\Delta_{2,b-1}, \Delta_{2,b})).$$

Define the threshold-vector estimate  $\widehat{\Delta}$  as

$$\widehat{\Delta}_{j,a} := \Phi^{-1}\left(\frac{1}{N} \sum_{i=1}^N \mathbb{I}(R_{i,j} \leq a)\right), \quad \forall a \in [C_j - 1], \quad j = 1, 2.$$

For population parameters  $\rho^*, \Delta_1^*, \Delta_2^*$ , define the sample and population loss functions as

$$\begin{aligned} \ell_N(\rho) &:= \frac{1}{N} \sum_{i=1}^N \log \pi_{R_{i,1}, R_{i,2}}(\rho; \widehat{\Delta}), \\ \ell_\infty(\rho) &:= \mathbb{E} \log \pi_{R_{i,1}, R_{i,2}}(\rho; \Delta^*) = \sum_{a \in [C_1], b \in [C_2]} \pi_{a,b}(\rho^*; \Delta^*) \log \pi_{a,b}(\rho; \Delta^*). \end{aligned}$$

Then, for  $\widehat{\rho}_N := \operatorname{argmax} \ell_N(\rho)$ , there exist absolute constants  $c_1, c_2, c_3 > 0$  (that only depend on  $C_1, C_2, \delta_1, \delta_2, M$ ) such that

$$\mathbb{P}(|\widehat{\rho}_N - \rho^*| > t) \leq c_1(e^{-c_2 N t^2} + e^{-c_3 N}), \quad \forall t > 0.$$

*Proof of Proposition 3.* We first prove the tail bound (13). Set  $E_1, E_2$  as before, so that

$\mathbb{P}(E_1^c) \leq Ke^{-cN/K}$ . On  $E_2$ , the estimator  $\widehat{\Sigma}_k$  is exactly the oracle estimator  $\widehat{\Sigma}_k^*$  computed using the true labels. Conditional on the labels, the oracle estimator for class  $k$  is based on  $N_k$  observations; hence, by applying Lemma 1 with  $N = N_k$ , we get

$$\mathbb{P}(\|\widehat{\Sigma}_k^* - \Sigma_k\|_{\max} > t, E_1) \leq c_1 J^2 \left( e^{-c_2 c N t^2 / K} + e^{-c_3 c N / K} \right)$$

for some constants  $c_1, c_2, c_3 > 0$ .

Hence, we can write

$$\begin{aligned} \mathbb{P}\left(\max_{k=1}^K \|\widehat{\Sigma}_k - \Sigma_k\|_{\max} > t\right) &\leq \mathbb{P}\left(\max_{k=1}^K \|\widehat{\Sigma}_k^* - \Sigma_k\|_{\max} > t\right) + \mathbb{P}(E_2^c) \\ &\leq \sum_{k=1}^K \mathbb{P}\left(\|\widehat{\Sigma}_k^* - \Sigma_k\|_{\max} > t, E_1\right) + \mathbb{P}(E_1^c) + \mathbb{P}(E_2^c) \\ &\leq c_1 K J^2 \left( e^{-c_2 N t^2 / K} + e^{-c_3 N / K} \right) + p_1, \end{aligned}$$

where the second line follows from a union bound, and  $p_1$  dominates  $\mathbb{P}(E_1^c)$  in the last line. By taking  $t := c\sqrt{\frac{K \log(JK)}{N}}$  with a large enough constant  $c$  and using the assumptions  $N/K \gtrsim \log(JK), p_1 = O(N^{-1})$ , the RHS becomes  $O((JK)^{-1} + N^{-1})$ .

□

*Proof of Proposition 4.* It suffices to show that the aggregated graph  $\mathbf{G}$  (defined by the binary matrix  $\mathbf{G}$ ) has no edges between distinct true blocks and contains the within-block connected components  $\cup_{\ell} E_{\ell}$  with high probability. To see why, recall that Assumption 1 assumed every true block  $V_{\ell}$  to be connected. The absence of cross-block edges implies that no connected component of  $\mathbf{G}$  can contain vertices from two different true blocks. Therefore, the connected components of  $\mathbf{G}$  are exactly  $V_1, \dots, V_L$ .

To show the claim, work on the high probability set  $F := \left\{ \max_{k=1}^K \|\widehat{\Sigma}_k - \Sigma_k\|_{\max} \leq \tau_1 \right\}$ . If  $j$  and  $j'$  belong to different true blocks, then  $\sigma_{(j,j'),k} = 0$  for all  $k \in [K]$  by the block-diagonal structure of  $\Sigma_k$ . On  $F$ , this implies  $|\widehat{\sigma}_{(j,j'),k}| \leq \tau_1$  for all  $k$ , and hence  $g_{j,j'} = 0$ . On the other hand, if  $\max_{k \in [K]} |\sigma_{(j,j'),k}| > \epsilon_N \geq 2\tau_1$ , then there exists some  $k \in [K]$  such that

$$|\widehat{\sigma}_{(j,j'),k}| \geq |\sigma_{(j,j'),k}| - \tau_1 > \tau_1.$$

Therefore,  $\max_{k \in [K]} |\widehat{\sigma}_{(j,j'),k}| > \tau_1$  and  $g_{j,j'} = 1$ . This proves the desired recovery of off-block zeros and within-block connected components.  $\square$

### B.3 Proof of results from Section 3.3

*Proof of Proposition 5.* (a) We work under the high probability event of correct block recovery given in Proposition 4. The conclusion follows from equation (13) in (Theorem 6, Cai et al., 2011). Here, we take  $\rho = 0$  and note that no parameter space assumptions are required for eq. (13) therein.

(b) This is immediate by part (a) and the additional assumption that  $\epsilon'_N \geq 8M'_N\lambda$ .  $\square$

## C Proof of Lemmas

To prove Lemma 1, we use the following two lemmas. The first lemma is a restatement of the usual MLE consistency argument (see Theorem 5.7 in Van der Vaart (2000)).

**Lemma 2.** *Fix any  $\epsilon > 0$ . Let  $\ell_N, \ell_\infty$  be functions and suppose there exists  $\eta = \eta(\epsilon)$  such that*

$$\mathbb{P}\left(\sup_{\rho} |\ell_N(\rho) - \ell_\infty(\rho)| > \eta\right) \leq p(\eta), \quad \ell_\infty(\rho^*) > \ell_\infty(\rho) + 2\eta$$

for all  $\rho$  with  $|\rho - \rho^*| \geq \epsilon$ . Then, we have  $|\widehat{\rho} - \rho^*| \leq \epsilon$  with probability  $1 - p(\eta)$ .

The second lemma is a technical result to ensure that the proportion parameter  $\pi_{a,b}$  and its derivative are well-defined and bounded. Its proof is postponed to the end of the section.

**Lemma 3.** *Assume that  $|\rho| \leq 1 - \delta_1$ ,  $\max_{a,b} (|\Delta_{1,a}|, |\Delta_{2,b}|) \leq M$ , and  $\min_{a,b} (|\Delta_{1,a} - \Delta_{1,a-1}|, |\Delta_{2,b} - \Delta_{2,b-1}|) \geq \delta_2$ . Here,  $a \in [C_1 - 1]$ ,  $b \in [C_2 - 1]$ .*

(a) *For some constant  $c = c(\delta_1, \delta_2, M) > 0$ , we have  $\pi_{a,b}(\rho; \mathbf{\Delta}) > c$ .*

(b) *For some constant  $L = L(\delta_1, \delta_2, M) > 0$ , we have  $0 < \frac{\partial \log \pi_{a,b}(\rho; \mathbf{\Delta})}{\partial \Delta_{1,a}} < L$ . Similar bounds for other derivatives also hold.*

*Proof of Lemma 1.* Throughout the proof, the lowercase  $c$  will denote absolute constants whose exact values may vary, and we shall omit the dependence on the values  $C_1, C_2, \delta_1, \delta_2, M$ . Following the notation convention, let  $\Delta = (\Delta_1^\top, \Delta_2^\top)^\top$ . Noting that  $\pi_{a,b}$  is bounded away from zero (see Lemma 3), both  $\partial_\rho^3 \ell$  and  $\partial_\rho^2 \partial_\Delta \ell$  are uniformly bounded above by some constants  $M_3 = M_3(\delta_1, \delta_2, M)$  and  $M_\Delta = M_\Delta(\delta_1, \delta_2, M)$ . Also, by direct computation, we get

$$-\ell''_\infty(\rho^*) = \sum_{a,b} \frac{\partial_\rho \pi_{a,b}(\rho^*; \Delta_1^*, \Delta_2^*)^2}{\pi_{a,b}(\rho^*; \Delta_1^*, \Delta_2^*)} \geq \frac{\phi_2(\Delta_{1,1}^*, \Delta_{2,1}^*; \rho^*)^2}{\pi_{1,1}(\rho^*; \Delta_1^*, \Delta_2^*)} := \kappa(\rho^*) > 0. \quad (19)$$

The inequality uses the summand corresponding to the index  $a = b = 1$ , and  $\kappa(\rho^*)$  is a positive constant that depends on the true parameters. Note that  $\kappa(\rho^*)$  can be further lower bounded by  $c(\delta_1, M)$  by a similar bound as in Lemma 3(a).

**Step 0. Preliminary error bounds.** In the remainder of the proof, we will work on the event

$$E_1 := \left\{ \|\widehat{\Delta} - \Delta\|_\infty \leq \frac{\kappa(\rho^*)}{6M_\Delta} \right\}, \quad E_2 := \left\{ |\widehat{\rho} - \rho^*| \leq \frac{\kappa(\rho^*)}{6M_3} \right\}. \quad (20)$$

We start by claiming that both events occur with exponentially high probability, that is,  $\mathbb{P}(E_1), \mathbb{P}(E_2) \geq 1 - O(e^{-cN})$ .

We first show the claim for  $E_1$ . This follows by applying the second conclusion in Proposition 2 with the choices  $K = 1, J = 2$  and  $t = \frac{\kappa(\rho^*)}{6M_\Delta}$  as in (20). Note that this choice of  $t$  is a constant, and is absorbed into the generic constant  $c$ .

Next, we move on to bounding  $E_2$ . By applying Lemma 2 with the choices  $\epsilon = \frac{\kappa(\rho^*)}{6M_3}$  and  $\eta = \eta(\epsilon)$ , it suffices to show the uniform law with  $p(\eta) = e^{-c(\eta)N}$ . For this goal, define

$$\ell_N^*(\rho) := \frac{1}{N} \sum_{i=1}^N \log \pi_{R_{i,1}, R_{i,2}}(\rho; \Delta^*)$$

and write

$$\mathbb{P}\left(\sup_\rho |\ell_N(\rho) - \ell_\infty(\rho)| \geq \eta\right) \leq \mathbb{P}\left(\sup_\rho |\ell_N(\rho) - \ell_N^*(\rho)| \geq \frac{\eta}{2}\right) + \mathbb{P}\left(\sup_\rho |\ell_N^*(\rho) - \ell_\infty(\rho)| \geq \frac{\eta}{2}\right)$$

$$\begin{aligned}
&\leq \mathbb{P}\left(\sup_{\rho} \sup_{a,b} |\log \pi_{a,b}(\rho; \widehat{\Delta}) - \log \pi_{a,b}(\rho; \Delta^*)| \geq \frac{\eta}{2}\right) + e^{-cN\eta^2} \\
&\leq \mathbb{P}\left(\|\widehat{\Delta} - \Delta^*\| \geq \frac{\eta}{2L}\right) + e^{-cN\eta^2} \lesssim e^{-cN\eta^2}.
\end{aligned} \tag{21}$$

Here, the first line uses a triangle inequality. The second line follows by noting that

$$\begin{aligned}
|\ell_N(\rho) - \ell_N^*(\rho)| &= \frac{1}{N} \left| \sum_{i=1}^N \sum_{a,b} \mathbb{I}(R_{i,1} = a, R_{i,2} = b) \left( \log \pi_{a,b}(\rho; \widehat{\Delta}) - \log \pi_{a,b}(\rho; \Delta^*) \right) \right| \\
&\leq \sup_{a,b} \left| \log \pi_{a,b}(\rho; \widehat{\Delta}) - \log \pi_{a,b}(\rho; \Delta^*) \right|
\end{aligned}$$

(for the first term in (21)), and the uniform version of Hoeffding's inequality (for the second term in (21)). The third line follows from noting that  $\log \pi_{a,b}(\rho; \cdot)$  is  $L$ -Lipschitz where  $L$  is uniform in  $a, b, \rho$  (see part (b) of Lemma 3), followed by the concentration result for  $\widehat{\Delta}$  in Proposition 2.

**Step 1. Score equation.** Define the score function (the derivative of  $\ell_N$ ) as

$$S_N(\rho, \widehat{\Delta}) := \frac{1}{N} \sum_{i=1}^N \partial_{\rho} \log \pi_{R_{i,1}, R_{i,2}}(\rho; \widehat{\Delta}_1, \widehat{\Delta}_2).$$

By definition, we have  $S_N(\widehat{\rho}, \widehat{\Delta}) = 0$ . By a Taylor expansion, we can write

$$0 = S_N(\rho^*, \Delta^*) + \partial_{\rho} S_N(\widetilde{\rho}, \widetilde{\Delta})(\widehat{\rho} - \rho^*) + \partial_{\Delta} S_N(\widetilde{\rho}, \widetilde{\Delta})^{\top}(\widehat{\Delta} - \Delta^*)$$

for some  $(\widetilde{\rho}, \widetilde{\Delta}) \in (\widehat{\rho}, \rho^*) \times (\widehat{\Delta}, \Delta^*)$ . Rearranging the terms, we get

$$\widehat{\rho} - \rho^* = -[\partial_{\rho} S_N(\widetilde{\rho}, \widetilde{\Delta})]^{-1} (S_N(\rho^*, \Delta^*) + \partial_{\Delta} S_N(\widetilde{\rho}, \widetilde{\Delta})^{\top}(\widehat{\Delta} - \Delta^*)). \tag{22}$$

In the remainder of the proof, we show that the denominator is bounded away from zero with probability  $1 - O(e^{-cN})$ , and that the numerator exhibits exponential concentration.

**Step 2. Bounding the denominator of (22).** We claim that  $\partial_{\rho} S_N(\widetilde{\rho}, \widetilde{\Delta}) \leq -\kappa(\rho^*)/3$  with probability greater than  $1 - O(e^{-cN})$ . By Step 0, we can work on the event  $E_1, E_2$  (see

(20)). For notational convenience, denote  $J_N := \partial_\rho S_N$ . As  $J_N$  is a continuous function on a compact set, we can write

$$|J_N(\tilde{\rho}, \tilde{\Delta}) - J_N(\rho^*, \Delta^*)| \leq M_3 |\tilde{\rho} - \rho^*| + M_\Delta \|\tilde{\Delta} - \Delta^*\| \leq \frac{\kappa(\rho^*)}{3}.$$

Here,  $M_3, M_\Delta$  denote the upper bounds of  $\partial_\rho^3 \ell, \partial_\rho^2 \partial_\Delta \ell$  as introduced in the beginning of the proof, and the final inequality follows as we are working under  $E_1, E_2$ .

Also, noting that  $\mathbb{E}J_N(\rho^*, \Delta^*) = \ell''_\infty(\rho^*) \leq -\kappa(\rho^*)$  (see (19)), Hoeffding's inequality gives that

$$\mathbb{P}\left(|J_N(\rho^*, \Delta^*) - \ell''_\infty(\rho^*)| > t\right) \lesssim e^{-cNt^2}.$$

By taking  $t = \kappa(\rho^*)/3$  and combining everything, we get

$$J_N(\tilde{\rho}, \tilde{\Delta}) \leq J_N(\rho^*, \Delta^*) + \frac{\kappa}{3} \leq \ell''_\infty(\rho^*) + \frac{2\kappa}{3} \leq -\frac{\kappa}{3}$$

with probability greater than  $1 - O(e^{-cN})$ . The constant  $c$  here can be made uniform in  $\rho^*$  by lower bounding  $\kappa = \kappa(\rho^*)$  with a constant that only depends on  $\delta_1, M$ .

**Step 3. Concentration for the numerator of (22).** We separately control the two terms in the numerator. For the first term, we use the following identity:

$$\mathbb{E}\partial_\rho \log \pi_{R_{i,1}, R_{i,2}}(\rho^*; \Delta^*) = 0.$$

This follows from using the definition of KL divergence to note that  $\ell_\infty$  is maximized at  $\rho^*$ , and re-writing  $\partial_\rho \ell_\infty(\rho^*) = 0$ . Writing  $S_N$  as the i.i.d. sum of bounded random variables:

$$S_N(\rho^*, \Delta^*) = \frac{1}{N} \sum_{i=1}^N \partial_\rho \log \pi_{R_{i,1}, R_{i,2}}(\rho^*; \Delta^*),$$

Hoeffding's inequality gives

$$\mathbb{P}(|S_N(\rho^*, \Delta^*)| > t) \lesssim e^{-cNt^2}.$$

For the second term in the numerator of (22), we use the concentration of  $\hat{\Delta} - \Delta$  in Proposition 2 and the fact that the derivatives  $\partial_\Delta S_N$  are bounded in the compact parameter

space to get

$$\mathbb{P}\left(|\partial_{\Delta} S_N(\tilde{\rho}, \tilde{\Delta})^\top(\hat{\Delta} - \Delta^*)| > t\right) \leq \mathbb{P}\left(\|\hat{\Delta} - \Delta^*\| > ct\right) \lesssim e^{-cNt^2}.$$

Note that we omit the dependence of  $C_1 + C_2$  in both inequalities.

The final conclusion is immediate by combining steps 2 and 3.  $\square$

*Proof of Lemma 3.* (a) Writing out the p.d.f. of  $(X_1, X_2)$  as

$$\phi_2(x_1, x_2; \rho) = \frac{1}{2\pi\sqrt{(1-\rho^2)}} e^{-\frac{x_1^2 - 2\rho x_1 x_2 + x_2^2}{2(1-\rho^2)}} \geq \frac{1}{2\pi} e^{-\frac{x_1^2 - 2\rho x_1 x_2 + x_2^2}{2(1-\rho^2)}},$$

it suffices to lower bound the exponential term.

For each category interval, choose a subinterval of length at least  $\delta_* := \min\{\delta_2, 1\} > 0$  that lies inside the category interval and inside  $[-M - 1, M + 1]$ . For interior categories, this follows from the separation condition; for the first and last categories, use the intervals adjacent to the finite boundary threshold. For any  $(x_1, x_2)$  in the resulting rectangle, we have

$$x_1^2 - 2\rho x_1 x_2 + x_2^2 \leq 4(M + 1)^2, \quad 1 - \rho^2 \geq 1 - (1 - \delta_1)^2 \geq \delta_1,$$

so  $-\frac{x_1^2 - 2\rho x_1 x_2 + x_2^2}{2(1-\rho^2)} \geq -\frac{2(M+1)^2}{\delta_1}$ . Then, the lower bound of  $\pi_{a,b}$  follows by integrating over this subrectangle:

$$\pi_{a,b}(\rho; \Delta_1, \Delta_2) = \int_{\Delta_{1,a-1}}^{\Delta_{1,a}} \int_{\Delta_{2,b-1}}^{\Delta_{2,b}} \phi_2(x_1, x_2; \rho) dx_2 dx_1 \geq \frac{\delta_*^2}{2\pi} e^{-\frac{2(M+1)^2}{\delta_1}} := c > 0.$$

(b) The lower bound 0 is immediate as  $\pi_{a,b}$  (as a function of  $\Delta_{1,a}$ ) is increasing in  $\Delta_{1,a}$ . By the chain rule and using the conclusion of part (a), we have

$$\begin{aligned} \frac{\partial \log \pi_{a,b}(\rho; \Delta)}{\partial \Delta_{1,a}} &= \frac{1}{\pi_{a,b}(\rho; \Delta)} \frac{\partial \pi_{a,b}(\rho; \Delta)}{\partial \Delta_{1,a}} \leq \frac{1}{c} \frac{\partial \pi_{a,b}(\rho; \Delta)}{\partial \Delta_{1,a}} \\ &= \frac{1}{c} \int_{\Delta_{2,b-1}}^{\Delta_{2,b}} \phi_2(\Delta_{1,a}, x_2; \rho) dx_2 \leq \frac{\phi(\Delta_{1,a})}{c} \leq \frac{1}{\sqrt{2\pi c}}. \end{aligned}$$

Here, the equality in the second line used the fundamental theorem of calculus, and the inequalities follow from relaxing the integration range. This completes the proof as we can

take  $L = 1/(\sqrt{2\pi c})$ . For other derivatives (such as with respect to  $\Delta_{1,a-1}$  when  $a > 1$ ), the partial derivative is still absolutely bounded by  $L$ .  $\square$

## D Simulation Details

### D.1 Data generation details

To generate the data for each simulation run, we first construct the block-diagonal precision matrices  $\mathbf{\Omega}_k$ . For each block, let  $\mathbf{B}$  be the adjacency matrix of the Erdős-Rényi random graph with probability  $s$ . Set each block precision matrix as  $\mathbf{\Omega}_k^{(\ell)} = 0.5\mathbf{B} + \delta\mathbf{I}$ , where  $\delta$  is dynamically chosen such that the condition number of the matrix is exactly equal to the block dimension  $M = J/L$ . Finally, we invert  $\mathbf{\Omega}_k^{(\ell)}$  to get the raw covariance matrix and rescale it so that  $\mathbf{\Sigma}_k$  is a correlation matrix with unit diagonals.

For each observation  $i$ , assume the class proportions are equal ( $\pi_k = 1/K$ ), and generate a latent class  $Z_i$  uniformly from  $[K]$ . Given a latent class assignment  $Z_i = k$ , we draw a continuous latent vector  $\mathbf{X}_i \sim \mathcal{N}(\mathbf{0}, \mathbf{\Sigma}_k)$ . We then discretize  $\mathbf{X}_i$  into the observed ordinal response vector  $\mathbf{R}_i$  using class-specific threshold parameters. For the binary items, we draw a single threshold  $\Delta_{j,1,k} \sim U[-1, 1]$ . For the four-category items, we draw three sorted thresholds  $(\Delta_{j,1,k}, \Delta_{j,2,k}, \Delta_{j,3,k})$  uniformly from  $[-2, 2]$ .

### D.2 Implementation choices for Step 3

**Precision matrix estimation** We implement the graphical lasso to estimate the precision matrices. When the covariance matrix estimate  $\widehat{\mathbf{\Sigma}}_k^{(\ell)}$  is not positive definite, we ensure this by appropriately increasing the diagonal elements. Later, in Appendix E.2, we conduct additional simulations comparing the graphical lasso with CLIME. They have similar accuracy, whereas the graphical lasso is much faster.

**Tuning parameter selection** For each simulation setting, we run 10 preliminary simulations to select the tuning parameter  $\lambda$  via cross-validation, as mentioned in Section 3.4.

We choose the most frequently selected value, which is often identical for all 10 trials. This selected  $\lambda$  is fixed throughout the main trials (100 replications). Below, we elaborate on the tuning parameter selection.

We randomly partition the dataset into  $F = 5$  folds of roughly equal sizes. For a given candidate tuning parameter  $\lambda$  from the grid  $\Lambda = \{0.1, 0.5, 1, 2\} \times \sqrt{\frac{\log(JK)}{N}}$ , we iteratively hold out each fold  $f \in \{1, \dots, F\}$  as the test set and use the remaining data as the training set. Let  $\widehat{\Sigma}_k^{(f)}$  be the estimated covariance matrix (estimated via Step 2) using only the observations from the  $f$ -th fold, and let  $\widehat{\Omega}_{k,\lambda}^{(-f)}$  denote the precision matrix estimate using the observations excluding the  $f$ -th fold (via Step 3).

We evaluate the performance of each candidate  $\lambda$  using the predictive negative Gaussian log-likelihood. The optimal tuning parameter is chosen by minimizing this validation loss aggregated across all  $K$  classes and  $F$  test folds:

$$\text{CV}(\lambda) = \sum_{f=1}^F \sum_{k=1}^K \widehat{N}_k^{(f)} \left[ \text{tr} \left( \widehat{\Sigma}_k^{(f)} \widehat{\Omega}_{k,\lambda}^{(-f)} \right) - \log \det \left( \widehat{\Omega}_{k,\lambda}^{(-f)} \right) \right],$$

where  $\widehat{N}_k^{(f)}$  denotes the number of observations assigned to the  $k$ -th cluster when holding out the  $f$ -th fold. After selecting the optimal tuning parameter  $\widehat{\lambda} = \arg \min_{\lambda \in \Lambda} \text{CV}(\lambda)$ , we finally run Step 3 to estimate  $\widehat{\Omega}$ .

### D.3 Guideline for selecting $K$

In the simulations, we assume that  $K$  is correctly specified. In general, the number of latent classes,  $K$ , is often unknown. In spectral clustering, one standard approach is the “elbow method,” which uses a scree plot (Thorndike, 1953; Ketchen and Shook, 1996). This procedure involves evaluating the k-means objective function (9) across a range of  $K$  values and selecting the “elbow” value where the decrease in clustering error flattens. Similarly, one can observe the largest gap/ratio among the singular values of the flattened data matrix  $\widetilde{\mathbf{R}}$ . Alternative methods include using information criteria (such as BIC or Extended BIC) after fitting the entire model for each  $K$ , or evaluating pointwise cohesion and separation

via the Silhouette score (Rousseeuw, 1987).

## E Additional Comparisons and Visualizations

### E.1 Improving clustering accuracy via likelihood refinement

We discuss and evaluate a refined clustering method based on the learned block structures. Note that our original Step 1 is a simple spectral clustering procedure that does not take into account the dependence structure within the data. Hence, we propose a one-step likelihood refinement that uses the estimated threshold vector  $\widehat{\Delta}$ , the block partition  $\widehat{V}$ , and the blockwise covariance matrices  $\widehat{\Sigma}_k^{(\ell)}$ . The refinement updates the class assignment by maximizing the blockwise ordinal likelihood:

$$\widehat{Z}_i^{\text{ref}} = \operatorname{argmax}_{1 \leq k \leq K} \prod_{\ell=1}^{\widehat{L}} \mathbb{P} \left( \mathbf{X}^{(\ell)} \in \prod_{j \in \widehat{V}_\ell} \left[ \widehat{\Delta}_{j, R_{i,j-1,k}}, \widehat{\Delta}_{j, R_{i,j,k}} \right) \mid \mathbf{X}^{(\ell)} \sim N \left( \mathbf{0}, \widehat{\Sigma}_k^{(\ell)} \right) \right),$$

where the product term denotes the rectangle corresponding to the observed ordinal response pattern  $R_{i,j}$  in block  $\ell$ .

We fix  $N = 1000$  and  $J = 100$ , and vary  $K, L$ , and  $s$ . Here  $s$  denotes the connectivity probability used when generating the precision matrix. To create a more challenging clustering setting, we reduce the separation among the threshold parameters compared to the values in Appendix D.1. Specifically, after generating the original threshold vectors  $\Delta_k$  as in Appendix D.1, we rescale them toward their across-class mean  $\bar{\Delta} = K^{-1} \sum_{k=1}^K \Delta_k$  by setting

$$\Delta'_k = \frac{1}{3} \bar{\Delta} + \frac{2}{3} \Delta_k.$$

We compare this one-step likelihood refinement against our Step 1 (the spectral clustering method without the refinement) and the usual locally independent LCM fitted by EM. For fair comparison, both the EM algorithm and the k-means in Step 1 use 10 random starts and a maximum of 100 iterations.

The results are reported in Table 4. The one-step likelihood refinement substantially

$J$	$K$	$L$	$s$	Err( $\hat{\mathbf{Z}}$ )			RMSE( $\hat{\boldsymbol{\pi}}$ )		
				Spec.	Refined	EM	Spec.	Refined	EM
100	5	5	0.6	4.2	0.9	1.5	0.013	0.013	0.013
			0.2	4.6	0.5	1.3	0.013	0.013	0.013
		10	0.6	4.0	0.4	1.4	0.011	0.011	0.011
			0.2	4.2	0.3	1.6	0.013	0.013	0.013
	10	5	0.6	19.2	9.3	12.9	0.009	0.009	0.013
			0.2	23.0	6.9	11.9	0.009	0.009	0.013
		10	0.6	18.7	4.6	9.0	0.009	0.009	0.011
			0.2	18.3	2.9	11.6	0.009	0.009	0.013

Table 4: Comparison of spectral clustering (Step 1), the one-step likelihood refinement, and the usual EM algorithm under local independence.

improves the initial spectral clustering labels across all considered settings. For instance, when  $K = 10$ , where the spectral initialization has noticeably larger clustering error, the refinement reduces the error by more than half. This supports the use of the estimated blockwise covariance structure after Step 1. This advantage is less apparent in terms of estimating the proportion parameters, as the RMSE values do not decrease.

Another interesting observation is that the naive EM algorithm performs reasonably well for clustering, despite being misspecified. We believe this is because the coordinate-wise likelihood  $\mathbb{P}(R_{i,j} | Z_i, \boldsymbol{\Delta}_j)$  remains somewhat robust under moderate local dependence, and the misspecified marginal likelihood may be informative for estimating the threshold vector  $\boldsymbol{\Delta}$ . In fact, one may also view the spectral clustering objective as a misspecified independent Gaussian likelihood. A related phenomenon of a misspecified MLE having satisfactory performance under Gaussian mixtures has been investigated in [Lee et al. \(2025\)](#). We note that the one-step refinement is better than EM in the reported settings, suggesting that incorporating the estimated dependence structure is indeed more beneficial.

## E.2 Comparison of graphical model selection methods

We conduct simulations by considering two procedures for the precision matrix in Step 3: graphical lasso and CLIME, while fixing  $J = 100$ . The results in Table 5 show that CLIME

and graphical lasso lead to broadly comparable accuracy for estimating the sparse precision matrices. Across the eight settings, the support recovery error  $\text{Err}_0(\hat{\Omega})$  and Frobenius error  $\text{Err}_F(\hat{\Omega})$  are of similar magnitude. In several settings CLIME gives slightly smaller errors, especially when  $L = 10$ . The ROC curves in Figure 8 also resemble Figure 3, and we draw similar conclusions when Steps 1 or 2 are omitted.

The main difference is computational: CLIME is noticeably slower than graphical lasso. The computational gap is more evident when  $L$  and  $K$  increase. For example, when  $(K, L) = (10, 10)$ , CLIME takes about 30 seconds on average, whereas graphical lasso takes only about 4 seconds. The computational burden of CLIME further increases in larger dimensions, say  $J = 500$ .

$J$	$K$	$L$	$s$	glasso			CLIME		
				$\text{Err}_0(\hat{\Omega})$	$\text{Err}_F(\hat{\Omega})$	time (s)	$\text{Err}_0(\hat{\Omega})$	$\text{Err}_F(\hat{\Omega})$	time (s)
100	5	5	0.6	0.084	0.104	2.4	0.088	0.111	9.8
			0.2	0.085	0.100	2.3	0.086	0.104	9.5
		10	0.6	0.035	0.088	2.5	0.034	0.084	16.5
			0.2	0.038	0.086	2.3	0.037	0.081	16.0
	10	5	0.6	0.090	0.112	4.1	0.091	0.108	18.6
			0.2	0.068	0.111	3.9	0.062	0.103	18.5
		10	0.6	0.045	0.088	4.1	0.041	0.093	30.7
			0.2	0.038	0.096	4.1	0.034	0.090	30.2

Table 5: Comparison of graphical lasso and CLIME for precision matrix estimation and computation time. Here, Steps 1 and 2 are identically implemented.

### E.3 Illustration of incorrectly estimated blocks

We visualize a typical instance of incorrect block recovery in Figure 9. The figure is analogous to Figure 2, but instead considers a more challenging simulation setting with lower signal and smaller block length. We see that  $\hat{L} = 9$  is underestimated because two of the true blocks are merged. In general, we observed  $\hat{L} \leq L$  as discussed in the main text (see Section 4). The underestimation of blocks potentially leads to a higher FDR, but is better in terms of TPR as opposed to overestimating (i.e., further partitioning a correct block).

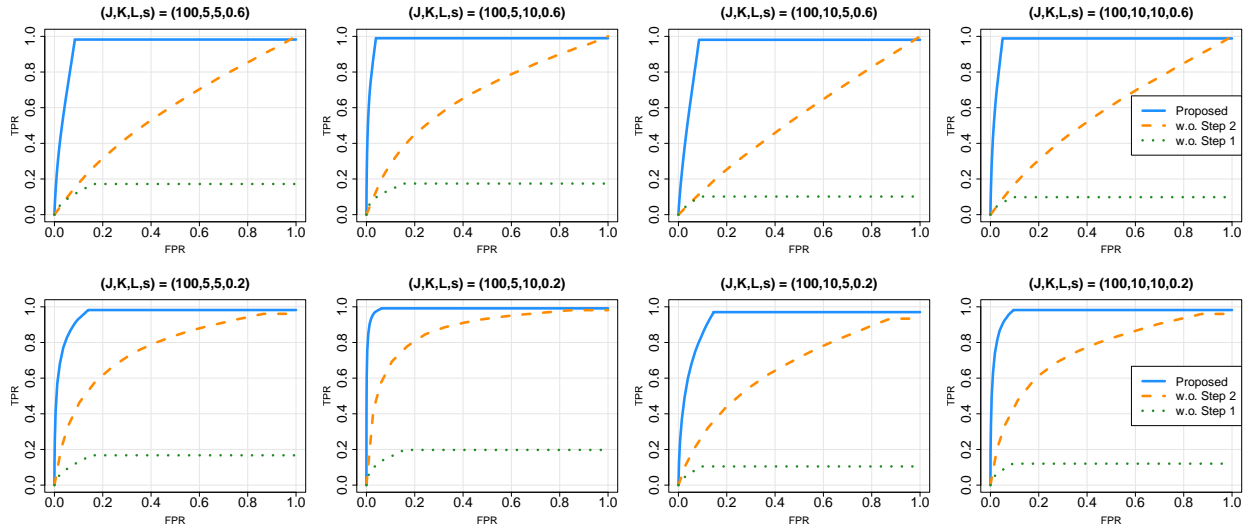


Figure 8: ROC curves for selecting  $\Omega$  under  $J = 100$  when the CLIME estimator is used. The solid line corresponds to the proposed method, whereas the dashed/dotted line corresponds to variants where Steps 2/1 are omitted, respectively.

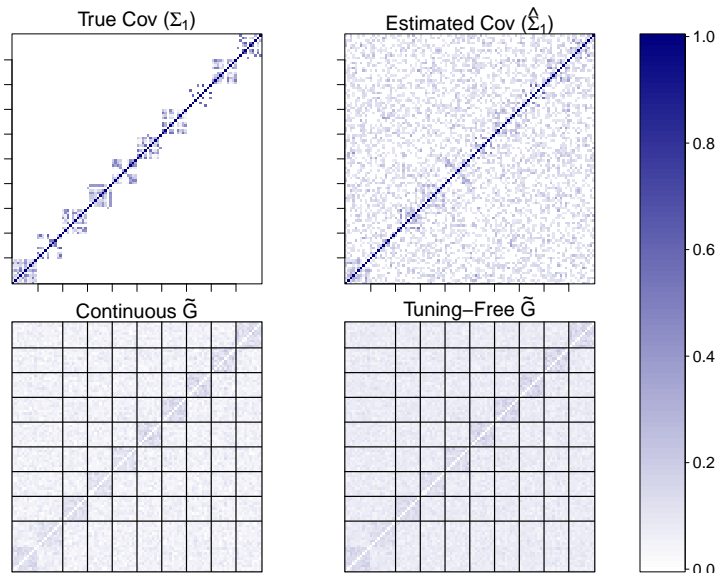


Figure 9: Analogue of Figure 2 under the challenging setting with parameters as in the 8th row of Table 1. While the true number of blocks is  $L = 10$ , the boundary between the first and second block is unclear. Thus, the Leiden algorithm selects  $\hat{L} = 9$  blocks where the true blocks indexed by  $\ell = 1, 2$  are merged.

## E.4 Tuning parameter sensitivity of our method and JGL

In Figure 10, we plot the average  $\hat{L}$  with respect to the tuning parameter, for both our method and JGL. We set  $K = L = 5$ ,  $s = 0.6$ . Our method is robust to the choice of

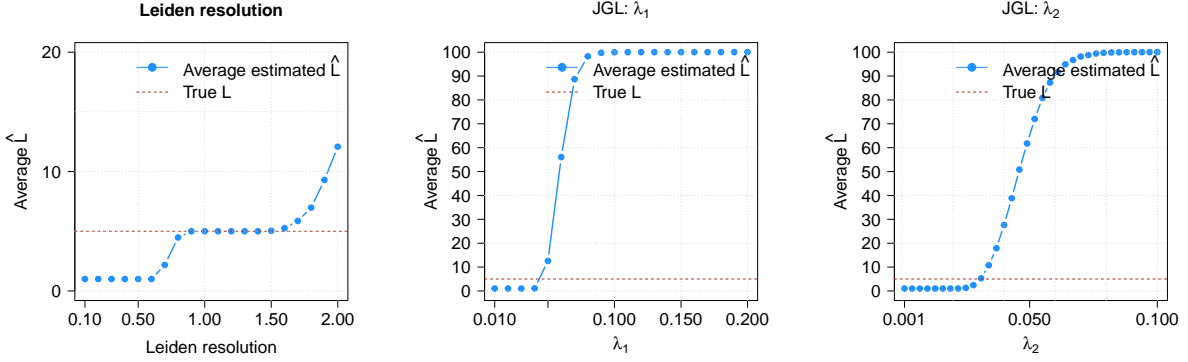


Figure 10: Sensitivity of the estimated number of blocks to tuning parameters. The left panel varies the Leiden resolution parameter, and the center/right panels vary the JGL parameters  $\lambda_1/\lambda_2$  (with the other parameter fixed at  $\lambda_2 = 0.001$  and  $\lambda_1 = 0.02$ , respectively). The horizontal dashed line marks the true number of blocks,  $L = 5$ . JGL is highly sensitive to the tuning choice, whereas the proposed Leiden-based block recovery is more robust to its resolution parameter.

resolution parameter, for a wide range of values from 0.8 to 1.5, which includes the default choice of 1. In other words, the proposed method performs well at a wide range of Leiden resolution parameters. In contrast, JGL is highly sensitive to its tuning parameters, and leads to uninformative block structures with  $\hat{L} = 1$  or  $J = 100$  for most values. We believe this instability is because the block structure learned by JGL is highly sensitive to false discovery. To elaborate, off-block-diagonal entries  $\sigma_{(j,j'),k}$  that are larger than the threshold in Theorem 2 in [Danaher et al. \(2014\)](#) (which depends on tuning parameters) result in merging the corresponding blocks.

This sensitivity made fully data-driven JGL tuning difficult in our experiments. Cross-validation and information criteria selected extreme block structures: CV, AIC, and BIC selected  $\hat{L} = 1$ , whereas EBIC selected  $\hat{L} = J$ . For example, CV selected  $\lambda_1 = 0.02, \lambda_2 = 0.0017$  which resulted in  $\hat{L} = 1$  blocks, which is why we additionally reported results under a more fine-tuned penalty in [Table 2](#). Fixing  $\lambda_2 = 0.001$  (larger values resulted in worse ARI), we chose  $\lambda_1 = 0.047$  so that the average  $\hat{L}$  is 5.1.

## F Real Data Analysis Details

### F.1 Implementation details

We provide further details on the implementation of each step of our method.

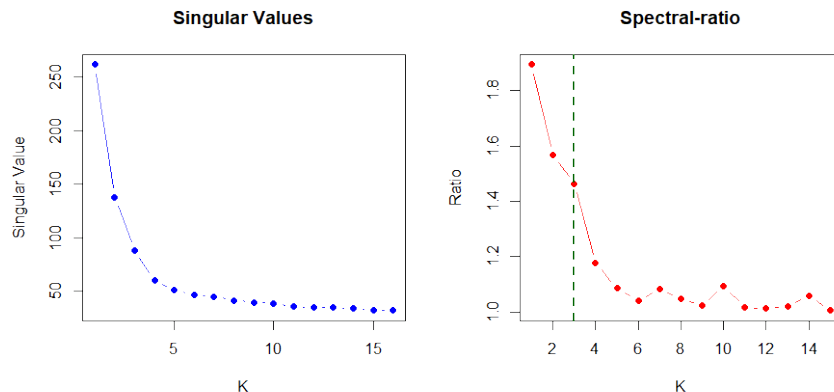


Figure 11: Visualization of the singular values and spectral ratios in the ANES data.

**Preprocessing** We preprocess the ANES data following [Chen et al. \(2026\)](#). We additionally remove one item that directly asks about the respondent’s party. The preprocessing details for the HapMap data are given in the main text.

**Step 1** For the ANES data, we selected  $K = 3$  mainly to match the interpretation of the three latent classes with political ideology. This is also supported by the spectral ratio, as  $K = 3$  corresponds to a rough elbow point in Figure 11. For the HapMap data, we selected  $K = 4$  to match the four subpopulations considered (Utah residents with European ancestry, Mexican ancestry in Los Angeles, Gujarati Indians in Houston, and Yoruba in Ibadan, Nigeria). Due to the numeric encoding of the responses (0, 1, 2), we implemented the clustering in Algorithm 1 directly on the raw data matrix  $\mathbf{R}$  without flattening. Note that we slightly abuse the notation, since the typical sample space for  $R_j$  with 3 categories is  $\{1, 2, 3\}$ .

**Step 2** In Step 2, we used the Leiden algorithm on the tuning-free version of the aggregated weight matrix  $\tilde{\mathbf{G}}$ . The high-resolution parameter value 1.5 is chosen based on the sensitivity analysis in Figure 10.

**Step 3 (for the ANES data)** In Step 3, we implemented graphical lasso. The tuning parameter  $\lambda = 0.3\sqrt{\log(JK)/N} = 0.019$  was selected by cross-validation, from the grid  $\Lambda = \{0.1, 0.3, 0.5, 1, 2\} \times \sqrt{\log(JK)/N}$ . We also tried selecting a separate  $\lambda_k$  per latent class, and the above value was selected for all classes.

## F.2 Additional visualization for the ANES data

We visualize the histogram of the number of categories  $C_j$  for all items in the ANES data in Figure 12. We see that  $C_j = 5$  is the most common, which typically takes ordered response categories “Not at all”-“A little”-“Somewhat”-“Very”-“Extremely”, or “Extremely important”-“Very important”-“Moderately important”-“Slightly important”-“Not at all important”. Items with  $C_j = 7$  typically arise when the voters are asked to rate on a scale of 1-7 without specific categories for the values 2-6. We also provide the details of the baseline block structures in Table 6, which were used to compute the ARI values for the estimated blocks. The block names provided here were also used as a rough guideline for interpreting the estimated blocks in Table 3.

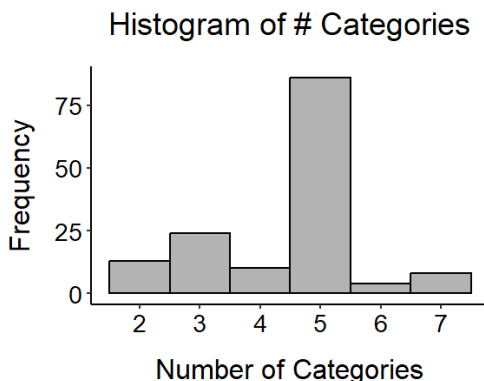


Figure 12: Histogram of the number of response categories  $C_j$  in the ANES dataset.

$\ell$	$J_\ell =  V_\ell $	Tag	$\ell$	$J_\ell =  V_\ell $	Tag
1	1	Follow politics	17	3	Guns and crime
2	1	Voter registration	18	6	Immigrant emotions
3	1	Turnout	19	9	Democratic attitudes
4	7	Participation	20	12	Electoral integrity
5	6	Global emotion	21	1	Political efficacy
6	3	Presidential approval	22	1	Racism
7	3	Economic performance	23	1	Feminist attitudes
8	8	Inflation	24	3	Political tolerance
9	14	Issue importance	25	11	Racial stereotypes
10	12	Issue ownership	26	2	Identities
11	1	Climate	27	5	Role of schools
12	1	Ukraine	28	1	Great replacement
13	4	Trust experts	29	4	Racial privilege
14	2	Political disagreement	30	2	Transgender attitudes
15	9	Abortion	31	4	Racial resentment
16	6	Abortion emotions	-	-	-

Table 6: The baseline block structure (with  $L = 31$  blocks) in the ANES questionnaire.

Next, in Table 7, we provide the exact item description for the 11 nodes that appear in Figure 6. While plotting Figure 6, we omitted edges whose weights are too small (defined by  $|\omega_{(j,j'),k}| < 3\lambda$ ) for better visibility. Without this thresholding, each  $\widehat{\Omega}_k$  has 41, 40, and 41 edges, of which 20 are shared. We also visualize the full  $\widehat{\Omega}_k$  (the  $144 \times 144$  matrix) in Figure 13, which illustrates the overall sparsity of the estimated precision matrices. Note that a negative precision matrix entry  $\omega_{(j,j'),k} < 0$  (colored in red) implies a positive partial correlation  $\rho_{(j,j'),k}$ , which is why the majority of the off-diagonal entries are red.

### F.3 Additional discussion for the HapMap3 data

We provide additional context for the problem of learning block structures in genetics. It is well understood that closely linked SNPs tend to exhibit stronger correlations (Gabriel et al., 2002). Commonly known as linkage disequilibrium (LD), this phenomenon naturally partitions the human genome into “haplotype blocks” of dependent SNPs, and learning such blocks has been an active area of research (Berisa and Pickrell, 2015; Yoo et al., 2015; Kim et al., 2018).

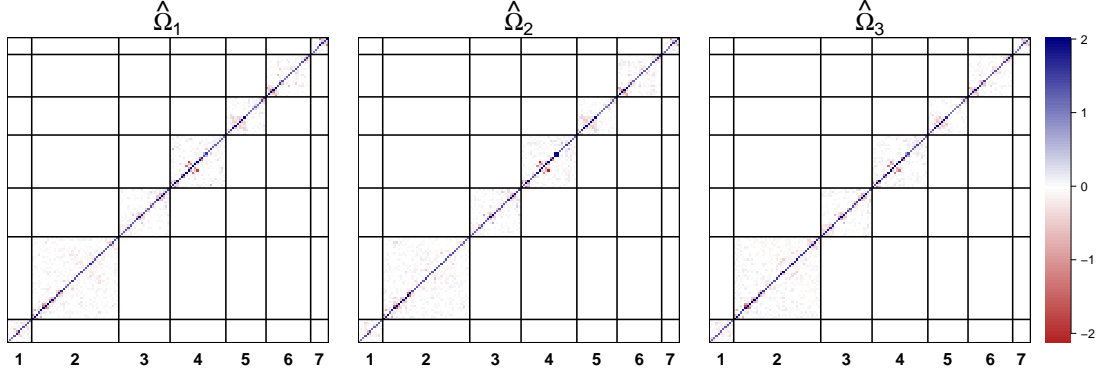


Figure 13: Visualization of the estimated precision matrices  $\hat{\Omega}_k$  for the ANES data. The elements are thresholded at  $\pm 2$  for better illustration.

Index	Variable Name	Questionnaire item
1	victimcrimebl	How worried are you about black citizens being the victims of violent crime?
2	victimpolicebl	How worried are you about black citizens being hurt or killed by the police?
3	rprob	In the United States, how serious a problem is racism?
4	nonwhite3	The demographic makeup of America is changing, with the U.S. Census Bureau estimating white people will become a minority. How do you feel?
5	whpriv	In American society, do you think that being White comes with advantages?
6	blpriv	In American society, do you think that being Black comes with advantages?
7	hipriv	In American society, do you think that being Hispanic comes with advantages?
8	aspriv	In American society, do you think that being Asian comes with advantages?
9	rr1	Irish, Italians, Jewish and many other minorities overcame prejudice and worked their way up. Blacks should do the same without any special favors.
10	rr2	Generations of slavery and discrimination have created conditions that make it difficult for Blacks to work their way out of the lower class.
11	rr3	Over the past few years, Blacks have gotten less than they deserve.

Table 7: Item identifiers and details for the visualization in Figure 6.

A common empirical strategy is to cluster SNPs using pairwise Pearson correlations,  $\text{Cor}(R_j, R_{j'})$ . This can be problematic in the presence of latent classes, as the correlations

induced by subpopulation differences may be mistaken for LD. Our analysis illustrates that the proposed method can learn block structure while accounting for unknown subpopulations. We note that some analyses estimate separate block structures for each subpopulation (Berisa and Pickrell, 2015). However, haplotype block boundaries are often similar across populations (Gabriel et al., 2002), which motivates our use of a shared block structure. Finally, we note that our modeling does not enforce the Hardy-Weinberg equilibrium (i.e., it does not assume that  $R_j \in \{0, 1, 2\}$  follows a binomial distribution), and allows for potential violations of this assumption.